Inorg. Chem. **2002**, *41*, 4872–4887

Modeling Substrate- and Inhibitor-Bound Forms of Liver Alcohol Dehydrogenase: Chemistry of Mononuclear Nitrogen/Sulfur-Ligated Zinc Alcohol, Formamide, and Sulfoxide Complexes

Magdalena M. Makowska-Grzyska,[†] Peter C. Jeppson,[†] Russell A. Allred,[†] Atta M. Arif,[‡] and Lisa M. Berreau*[,†]

Department of Chemistry and Biochemistry, Utah State University, Logan, Utah 84322-0300, and Department of Chemistry, University of Utah, Salt Lake City, Utah 84112

Received February 22, 2002

Using a mixed nitrogen/sulfur ligand possessing a single internal hydrogen bond donor (*N,N*-bis-2-(methylthio)-ethyl-*N*-(6-amino-2-pyridylmethyl)amine (bmapa)), we prepared and structurally and spectroscopically characterized a series of zinc complexes possessing a single alcohol ([(bmapa)Zn(MeOH)]$(ClO_4)_2$ (**1**)), formamide ([(bmapa)Zn-(DMF)]$(ClO_4)_2$ (**3**), [(bmapa)Zn(NMF)]$(ClO_4)_2$ (**4**)), or sulfoxide ([(bmapa)Zn(DMSO)]$(ClO_4)_2$ (**7**), [(bmapa)Zn(TMSO)]-$(ClO_4)_2$ (**8**)) ligand. X-ray crystallographic characterization was obtained for **1·MeOH**, **3**, **4**, **7·DMSO**, and **8**. To enable studies of the influence of the single hydrogen bond donor amino group of the bmapa ligand on the chemistry of zinc/neutral oxygen donor binding interactions, analogous alcohol ([(bmpa)Zn(MeOH)]$(ClO_4)_2$ (**2**)), formamide ([(bmpa)Zn(DMF)]$(ClO_4)_2$ (**5**), [(bmpa)Zn(NMF)]$(ClO_4)_2$ (**6**)), and sulfoxide ([(bmpa)Zn(DMSO)]$(ClO_4)_2$ (**9**), [(bmpa)-Zn(TMSO)]$(ClO_4)_2$ (**10**)) complexes of the bmpa (*N,N*-bis-2-(methylthio)ethyl-*N*-(2-pyridylmethyl)amine) ligand system were generated and characterized. Of these, **2**, **5**, **6**, and **9·2DMSO** were characterized by X-ray crystallography. Solution spectroscopic methods (^{1}H and ^{13}C NMR, FTIR) were utilized to examine the formamide binding properties of **3**–**6** in CH_3CN and CH_3NO_2 solutions. Conclusions derived from this work include the following: (1) the increased donicity of formamide and sulfoxide donors (versus alcohols) makes these competitive ligands for a cationic N/S-ligated zinc center, even in alcohol solution, (2) the inclusion of a single internal hydrogen bond donor, characterized by a heteroatom distance of ∼2.80–2.95 Å, produces subtle structural perturbations in N/S-ligated zinc alcohol, formamide, or sulfoxide complexes, (3) the heteroatom distance of a secondary hydrogen-bonding interaction involving the oxygen atom of a zinc-coordinated alcohol, formamide, and sulfoxide ligand is reduced with increasing donicity of the exogenous ligand, and (4) formamide displacement on a N/S-ligated zinc center is rapid, regardless of the presence of an internal hydrogen bond donor. These results provide initial insight into the chemical factors governing the binding of a neutral oxygen donor to a N/S-ligated zinc center.

Introduction

Mononuclear nitrogen/sulfur-ligated zinc centers are found within the active site of several metalloenzymes including liver alcohol dehydrogenase (LADH).[1] In LADH (Scheme 1),[2] the catalytic cycle is initiated via displacement of one neutral oxygen donor ligand (water) by another (the alcohol substrate) at the active site zinc ion. The results of recent synthetic modeling studies by Vahrenkamp et al.[3] and Parkin et al.[4] have suggested that the sulfur-containing zinc coordination environment in LADH may promote alcohol (versus water) binding. Notably, other neutral oxygen donor molecules are also known to bind to the active site zinc ion in LADH. For example, as the product of oxidation of a primary and secondary alcohol, an aldehyde or ketone likely transiently binds to the zinc center in LADH prior to displacement by water (Scheme 1) during catalytic turnover. Neutral

* Corresponding author. E-mail: berreau@cc.usu.edu. Phone: (435) 797-1625. Fax: (435) 797-3390.
[†] Utah State University.
[‡] University of Utah.

(1) Eklund, H.; Brändén, C.-I. In *Zinc Enzymes*; Spiro, T. G., Ed.; Wiley: New York, 1983; pp 124−152.
(2) Klinman, J. P. *Crit. Rev. Biochem.* **1981**, *10*, 39−78.
(3) Seebacher, J.; Shu, M.; Vahrenkamp, H. *Chem. Commun.* **2001**, 1026−1027.
(4) Kimblin, C.; Bridgewater, B. M.; Churchill, D. G.; Parkin, G. *Chem. Commun.* **1999**, 2301−2302.

10.1021/ic0255609 CCC: $22.00
Published on Web 08/20/2002

Scheme 1. Proposed Catalytic Cycle of Horse Liver Alcohol Dehydrogenase

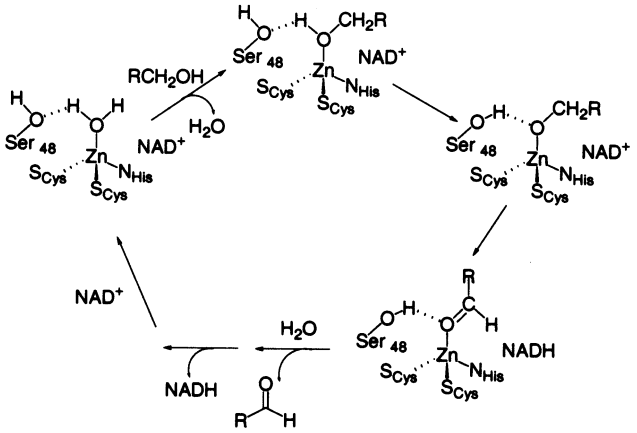

oxygen donor molecules that are structurally related to aldehydes/ketones are uncompetitive inhibitors[5] of LADH and bind to the enzyme−NADH complex. Compounds of this class include formamides[6] and sulfoxides,[7] whose interaction with the active site zinc ion has been determined by X-ray crystallography. Notably, formamide- and sulfoxide-inhibited forms of LADH remain catalytically inactive even in the presence of saturating amounts of alcohol.

Beyond the synthetic modeling studies by Vahrenkamp and Parkin mentioned previously, at this point, there is little chemical precedent on which to propose hypotheses regarding how the primary and secondary coordination environment of the active site zinc ion in LADH influences the binding of various neutral oxygen donor ligands. However, a recent study involving calixarene-based systems is noteworthy and relevant to the chemistry of LADH.[8] Reinaud et al. demonstrated that an N_3-ligated cationic zinc center, encapsulated in a calixarene ligand, forms stable complexes possessing a single bound alcohol or formamide ligand. The binding of these neutral oxygen donors to the cationic zinc center was stabilized through secondary hydrogen-bonding and CH/π interactions. In regard to hydrogen-bonding, one secondary structural moiety in LADH that must be considered is Ser_{48} (Figure 1), a polar residue that is located near the active site zinc ion and is known from X-ray crystallography to participate in hydrogen-bonding interactions with zinc-bound neutral oxygen donor ligands. For example, in alcohol-bound

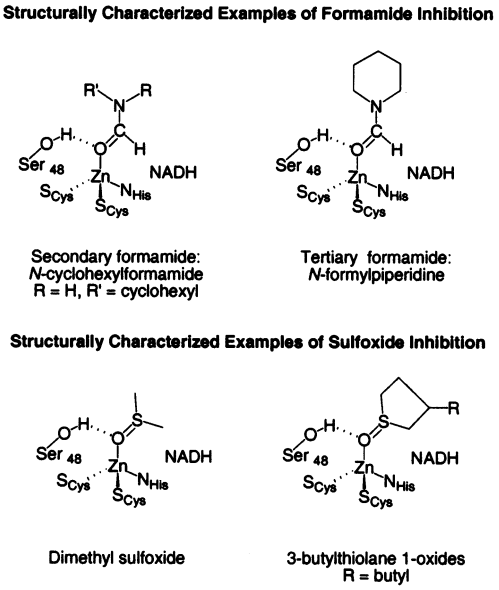

Figure 1. Inhibitor-bound forms of LADH with hydrogen-bonding interactions involving Ser_{48}.

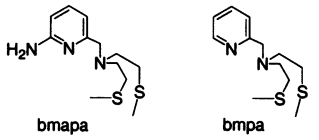

Figure 2. Ligands employed for synthesis of zinc alcohol, formamide, and sulfoxide complexes.

forms of the enzyme, Ser_{48} accepts a hydrogen bond from the zinc-bound alcohol (Scheme 1).[9] Structurally characterized forms of LADH possessing a zinc-bound formamide or sulfoxide inhibitor (Figure 1) are consistent with Ser_{48} donating a hydrogen bond to the zinc-bound oxygen atom of the inhibitor.[6,7] To what degree this hydrogen-bonding interaction influences the binding of a neutral oxygen donor molecule to the zinc center remains to be elucidated.

Recently, we reported the use of a new ligand system, bmapa (Figure 2, left), for modeling aspects of the active site chemistry of liver alcohol dehydrogenase.[10] This novel ligand provides a mixed nitrogen/sulfur metal coordination environment and a single internal hydrogen bond donor strategically positioned so as to enable the formation of a hydrogen bond with a ligand bound to the mononuclear zinc center. Our initial report demonstrated that mononuclear nitrogen/sulfur-ligated zinc alcohol and formamide complexes could be generated using this ligand system. We demonstrate herein that the bmapa ligand system enables the isolation of an entire family of complexes relevant to substrate- and inhibitor-bound forms of LADH. In addition, we display herein our ability to utilize a related ligand (bmpa, Figure 2, right) to begin to directly assess the influence of a single hydrogen bond donor on the neutral oxygen donor binding properties of a nitrogen/sulfur-ligated zinc center. The results derived from this work provide initial insight

(5) Plapp, B. V.; Chadha, V. K.; Leidal, K. G.; Cho, H.; Scholze, M.; Schindler, J. F.; Berst, K. B.; Ramaswamy, S. *Enzymol. Mol. Biol. Carbonyl Metab.* **1999**, *7*, 295−303.

(6) (a) Ramaswamy, S.; Scholze, M.; Plapp, B. V. *Biochemistry* **1997**, *36*, 3522−3527. (b) Schindler, J. F.; Berst, K. B.; Plapp, B. V. *J. Med. Chem.* **1998**, *41*, 1696−1701. (c) Porter, C. C.; Titus, D. C.; DeFelice, M. J. *Life Sci.* **1976**, *18*, 953−959. (d) Winer, A. D.; Theorell, H. *Acta Chem. Scand.* **1960**, *14*, 1729−1742. (e) Sigman, D. S. *J. Biol. Chem.* **1967**, *242*, 3815−3824. (f) Sarma, R. H.; Woronick, C. L. *Biochemistry* **1972**, *11*, 170−179. (g) Chadha, V. K.; Leidal, K. G.; Plapp, B. V. *J. Med. Chem.* **1983**, *26*, 916−922. (h) Delmas, C.; de Saint Blanquat, G.; Freudenreich, C.; Biellmann, J. F. *Alcohol. Clin. Exp. Res.* **1983**, *7*, 264−270.

(7) (a) Cho, H.; Plapp, B. V. *Biochemistry* **1998**, *37*, 4482−4489. (b) Cho, H.; Ramaswamy, S.; Plapp, B. V. *Biochemistry* **1997**, *36*, 382−389. (c) Chadha, V. K.; Leidal, K. G.; Plapp, B. V. *J. Med. Chem.* **1983**, *26*, 916−922. (d) Chadha, V. K.; Leidal, K. G.; Plapp, B. V. *J. Med. Chem.* **1985**, *28*, 36−40.

(8) Sénèque, O.; Giorgi, M.; Reinaud, O. *Chem. Commun*. **2001**, 984−985.

(9) Ramaswamy, S.; Eklund, H.; Plapp, B. *Biochemistry* **1994**, *33*, 5230−5237.

(10) Berreau, L. M.; Makowska-Grzyska, M. M.; Arif, A. M. *Inorg. Chem.* **2001**, *40*, 2212−2213.

into the chemical factors governing the binding of a neutral oxygen donor to a N/S-ligated zinc center.

Experimental Section

General Methods. All reagents and solvents were obtained from commercial sources and were used as received unless otherwise noted.

Physical Methods. FTIR spectra were recorded on a Shimadzu FTIR-8400 spectrometer as KBr pellets or solutions between NaCl plates. A table listing FTIR features of the new zinc complexes generated herein is available in the Supporting Information (Table S1). ^{1}H and ^{13}C{^{1}H} NMR spectra were recorded at 20(1) °C on a JEOL GSX-270 or Bruker ARX-400 spectrometer. Chemical shifts (in ppm) are referenced to the residual solvent peak(s) in CD_3CN (^{1}H, 1.95 (quintet); ^{13}C{^{1}H}, 1.39 (heptet) ppm). Tables listing the ^{1}H and ^{13}C NMR data for the new zinc complexes generated herein are available in the Supporting Information (Tables S2 and S3). Elemental analyses were performed by Atlantic Microlabs of Norcross, GA.

Caution! Perchlorate salts of metal complexes with organic ligands are potentially explosive. Only small amounts of material should be prepared, and these should be handled with great care.[11]

Synthesis of Ligands and Complexes. The ligand bmapa and the zinc complexes [(bmapa)Zn(MeOH)]$(ClO_4)_2$ (**1**) and [(bmapa)-Zn(DMF)]$(ClO_4)_2$ (**3**) were prepared as previously reported.[10]

***N,N*-Bis-2-(methylthio)ethyl-*N*-(2-pyridylmethyl)amine (bmpa).**[12] To a solution of 2-aminomethylpyridine (2.21 g, 0.0205 mol) in CH_3CN (100 mL) was added 1-bromo-2-methylthioethane (6.34 g, 0.0409 mol), sodium carbonate (7.91 g), and tetrabutylammonium bromide (∼3 mg). The resulting mixture was heated at reflux for 12 h under a N_2 atmosphere. After cooling to room temperature, the reaction mixture was poured into 1 M NaOH (∼100 mL). The resulting solution was extracted with CH_2Cl_2 (3 × ∼120 mL), the combined organic fractions were dried over Na_2SO_4, and the solution was brought to dryness under reduced pressure. Column chromatography on silica gel (ethyl acetate, $R_f \approx 0.64$) yielded the product as a pale yellow oil (2.88 g, 55%).

[(bmpa)Zn(CH$_3$OH)](ClO$_4$)$_2$ (2). To a methanol solution (5 mL) of bmpa (41 mg, 0.16 mmol) was added a methanol solution (5 mL) of $Zn(ClO_4)_2 \cdot 6H_2O$ (60 mg, 0.16 mmol). The resulting clear, pale yellow solution was stirred at ambient temperature for 20 min. An excess of diethyl ether (∼80 mL) was then added, and the resulting cloudy solution was cooled to ∼−28 °C for 12 h. A white solid that deposited was then collected and carefully dried under vacuum. Recrystallization of the product from diethyl ether diffusion into a ^{i}PrOH/CH_3OH (1:4) solution yielded colorless crystalline blocks suitable for X-ray diffraction analysis (58 mg, 66%). Anal. Calcd for $C_{13}H_{24}N_2S_2Cl_2O_9Zn$: C, 28.37; H, 4.40; N, 5.09. Found: C, 27.86; H, 4.41; N, 5.17.

[(bmapa)Zn(NMF)](ClO$_4$)$_2$ (4). To a solution of bmapa (43 mg, 0.16 mmol) in MeOH (3 mL) was added a methanol solution (3 mL) of $Zn(ClO_4)_2 \cdot 6H_2O$ (60 mg, 0.16 mmol). The resulting mixture was stirred for 15 min at which point *N*-methylformamide (18 μL, 0.32 mmol) was added and the resulting solution was stirred for an additional 20 min. The clear solution was then added to diethyl ether (∼40 mL), which resulted in the immediate precipitation of a white solid. Additional material precipitated after allowing the solution to stand at ∼−18 °C for 12 h. All white solid that had deposited was then collected and carefully dried under vacuum. Recrystallization from ^{i}PrOH/CH_3NO_2/Et_2O yielded pure product as colorless crystalline prisms suitable for X-ray crystallographic analysis (65 mg, 70%). Anal. Calcd for $C_{14}H_{26}N_4S_2Cl_2O_9Zn$: C, 28.38; H, 4.43; N, 9.46. Found: C, 28.56; H, 4.48; N, 9.44.

[(bmpa)Zn(DMF)](ClO$_4$)$_2$ (5). To a methanol solution (5 mL) of bmpa (46 mg, 0.18 mmol) was added a methanol solution (5 mL) of $Zn(ClO_4)_2 \cdot 6H_2O$ (66 mg, 0.18 mmol). The resulting clear, colorless solution was stirred at ambient temperature for 15 min. To this solution was added DMF (21 μL, 0.27 mmol), and the resulting solution was stirred for an additional 20 min. To this mixture was added excess diethyl ether (∼80 mL), and the resulting cloudy solution was cooled to ∼−28 °C for 12 h. A white solid that deposited was then collected and carefully dried under vacuum. Recrystallization of this powder from diethyl ether diffusion into a ^{i}PrOH/CH_3OH (1:5) solution yielded colorless crystalline blocks suitable for X-ray diffraction (72 mg, 68%). Anal. Calcd for $C_{15}H_{27}N_3S_2O_9Cl_2Zn$: C, 30.46; H, 4.60; N, 7.11. Found: C, 30.70; H, 4.69; N, 6.93. We note that ^{1}H NMR spectra of all isolated samples of **5** indicate a small amount of CH_3OH (<0.1 mol equiv) present that cannot be removed by drying under vacuum at ambient temperature. This may indicate the presence of a small amount of compound **2** (<10%) in isolated samples of **5**.

[(bmpa)Zn(NMF)](ClO$_4$)$_2$ (6). To a CH_3NO_2 slurry (2 mL) of $Zn(ClO_4)_2 \cdot 6H_2O$ (66 mg, 0.18 mmol) was added a CH_3NO_2 solution (5 mL) of bmpa (45 mg, 0.18 mmol). The mixture was stirred at ambient temperature until all of the zinc starting material had dissolved (∼15 min). To this solution was added NMF (21 μL, 0.35 mmol), and the resulting solution was stirred for an additional 10 min. To this mixture was added excess diethyl ether (∼80 mL), and the resulting cloudy solution was cooled to ∼−28 °C for 12 h. A white solid that deposited was then collected and carefully dried under vacuum. Recrystallization of this powder from diethyl ether diffusion into a ^{i}PrOH/CH_3NO_2 (1:2) solution yielded colorless crystalline blocks suitable for X-ray diffraction (64 mg, 63%). Anal. Calcd for $C_{14}H_{25}N_3S_2O_9Cl_2Zn$: C, 29.12; H, 4.37; N, 7.28. Found: C, 29.22; H, 4.30; N, 7.15.

[(bmapa)Zn(DMSO)](ClO$_4$)$_2$ (7). To a methanol solution (5 mL) of bmapa (48 mg, 0.18 mmol) was added a methanol solution (5 mL) of $Zn(ClO_4)_2 \cdot 6H_2O$ (66 mg, 0.18 mmol). The resulting clear, colorless solution was stirred at ambient temperature for 15 min. To this solution was added DMSO (18 μL, 0.27 mmol), and the resulting solution was stirred for an additional 20 min. The clear solution was then added to diethyl ether (∼100 mL), which resulted in the immediate precipitation of a white solid. Additional material precipitated after allowing the solution to stand at ∼−18 °C for 12 h. All white solid that deposited was then collected and carefully dried under vacuum. Recrystallization of this powder from Et_2O diffusion into a CH_3OH solution yielded a polycrystalline solid (78 mg, 72%). Anal. Calcd for $C_{14}H_{27}N_3S_3O_9Cl_2Zn$: C, 27.50; H, 4.45; N, 6.88. Found: C, 27.53; H, 4.36; N, 6.89. Recrystallization from diethyl ether diffusion into a DMSO:CH_3OH (1:15) solution yielded [(bmapa)Zn(DMSO)$_2$](ClO$_4$)$_2$ (**7·DMSO**) as colorless crystalline blocks suitable for X-ray diffraction (69%). Anal. Calcd for $C_{16}H_{33}N_3S_4O_{10}Cl_2Zn$: C, 27.87; H, 4.83; N, 6.10. Found: C, 28.16; H, 4.91; N, 6.17.

[(bmapa)Zn(d_6-DMSO)](ClO$_4$)$_2$ (7-d_6). Prepared and isolated using procedures similar to those employed for [(bmapa)Zn-(DMSO)](ClO$_4$)$_2$ except using d_6-DMSO.

[(bmapa)Zn(TMSO)](ClO$_4$)$_2$ (8). To a methanol solution (3 mL) of bmapa (33 mg, 0.12 mmol) was added a methanol solution (3

(11) Wolsey, W. C. *J. Chem. Educ.* **1973**, *50*, A335−A337.

(12) A slightly lower yield (49%) preparation for this ligand has been previously reported starting from vinylpyridine and *N,N*-bis(2-methylthioethyl)amine: Ambundo, E. A.; Deydier, M.-V.; Grall, A. J.; Aguera-Vega, N.; Dressel, L. T.; Cooper, T. H.; Heeg, M. J.; Orchrymowicz, L. A.; Rorabacher, D. B. *Inorg. Chem.* **1999**, *38*, 4233−4242.

mL) of $Zn(ClO_4)_2 \cdot 6H_2O$ (46 mg, 0.12 mmol). The resulting clear, colorless solution was stirred at ambient temperature for 15 min. To this solution was added tetramethylene sulfoxide (TMSO) (11 μL, 0.12 mmol), and the resulting solution was stirred for an additional 20 min. The clear solution was then added to diethyl ether (~80 mL), which resulted in the immediate precipitation of a white solid. Additional material precipitated after allowing the solution to stand at ~−18 °C for 12 h. All white solid that deposited was then collected and carefully dried under vacuum. Recrystallization of this powder from diethyl ether diffusion into a CH_3OH solution yielded colorless crystalline plates suitable for X-ray diffraction (55 mg, 70%). Anal. Calcd for $C_{16}H_{29}N_3S_3O_9Cl_2Zn$: C, 30.14; H, 4.59; N, 6.60. Found: C, 30.23; H, 4.56; N, 6.69.

[(bmpa)Zn(DMSO)](ClO$_4$)$_2$ (9). To a methanol solution (3 mL) of bmpa (59 mg, 0.23 mmol) was added a methanol solution (3 mL) of $Zn(ClO_4)_2 \cdot 6H_2O$ (85 mg, 0.23 mmol). The resulting clear, colorless solution was stirred at ambient temperature for 15 min. To this solution was added DMSO (25 μL, 0.35 mmol), and the resulting solution was stirred for an additional 20 min. To this mixture was added excess diethyl ether (~80 mL), and the resulting cloudy solution was cooled to ~−28 °C for 12 h. A white solid that deposited was then collected and carefully dried under vacuum. Recrystallization of this powder from diethyl ether diffusion into a CH_3OH solution led to the deposition of the product as a white polycrystalline material (98 mg, 71%). Anal. Calcd for $C_{14}H_{26}N_2S_3O_9Cl_2Zn$: C, 28.19; H, 4.40; N, 4.70. Found: C, 28.05; H, 4.44; N, 4.76. Recrystallization from diethyl ether diffusion into a DMSO/CH_3OH (1:10) solution yielded $[(bmpa)Zn(DMSO)_3](ClO_4)_2$ (**9·2DMSO**) as colorless crystalline blocks suitable for X-ray diffraction (69%). Anal. Calcd for $C_{16}H_{33}N_3S_4O_{10}Cl_2Zn$: C, 28.72; H, 5.09; N, 3.72. Found: C, 28.39; H, 5.13; N, 3.70.

[(bmpa)Zn(TMSO)](ClO$_4$)$_2$ (10). To a methanol solution (3 mL) of bmpa (48 mg, 0.18 mmol) was added a methanol solution (3 mL) of $Zn(ClO_4)_2 \cdot 6H_2O$ (68 mg, 0.18 mmol). The resulting reaction mixture was stirred at ambient temperature for ~15 min. To this solution was added tetramethylene sulfoxide (TMSO) (17 μL, 0.18 mmol), and the resulting solution was stirred for an additional 20 min. The clear solution was then added to diethyl ether (~120 mL), and the resulting cloudy solution was cooled to ~−28 °C for 12 h. A white solid that deposited was then collected and carefully dried under vacuum. Recrystallization of this powder from diethyl ether diffusion into a ^{i}PrOH/CH_3NO_2 (1:5) solution yielded colorless blocks (80 mg, 70%). Anal. Calcd for $C_{16}H_{28}N_2S_3O_9Cl_2Zn$: C, 30.87; H, 4.54; N, 4.50. Found: C, 30.85; H, 4.50; N, 4.52.

[(bmapa)Zn(CH$_3$CN)](ClO$_4$)$_2$ (11). To an acetonitrile solution (5 mL) of bmapa (43 mg, 0.16 mmol) was added an acetonitrile solution (5 mL) of $Zn(ClO_4)_2 \cdot 6H_2O$ (58 mg, 0.16 mmol). The resulting clear, yellowish solution was stirred at ambient temperature for 40 min. An excess of diethyl ether (~80 mL) was then added, and the resulting cloudy solution was cooled to ~−28 °C for 12 h. A white solid that deposited was then collected and carefully dried under vacuum. Recrystallization of the product from diethyl ether diffusion into a ^{i}PrOH/CH_3CN (1:5) solution yielded colorless crystalline blocks suitable for X-ray diffraction analysis (48 mg, 53%). Anal. Calcd for $C_{12}H_{21}N_3S_2Cl_2O_8Zn \cdot 0.66CH_3CN$: C, 28.56; H, 4.14; N, 9.16. Found: C, 28.49; H, 4.18; N, 9.22. The presence of $^2/_3$ of a molecule of CH_3CN in the analytical sample was corroborated by ^{1}H NMR analysis of the same sample.

[(bmapa)Zn(ClO$_4$)](ClO$_4$) (12). To a CH_3NO_2 slurry (3 mL) of $Zn(ClO_4)_2 \cdot 6H_2O$ (77 mg, 0.21 mmol) was added a CH_3NO_2 solution (3 mL) of bmapa (56 mg, 0.21 mmol). The mixture was stirred at ambient temperature until all of the zinc starting material had dissolved (~15 min) and then for an additional 20 min. This solution was then added to excess diethyl ether (~100 mL), and the resulting cloudy solution was cooled to ~−28 °C for 12 h. A white solid that deposited was then collected and carefully dried under vacuum. Recrystallization of the product from diethyl ether diffusion into a ^{i}PrOH/CH_3NO_2 (1:5) solution yielded colorless crystalline material deposited in a thick pale yellow oil. Drying of this combined material yielded 55 mg of a powdery white solid. ^{1}H NMR analysis of this powder indicated the presence of ~0.70 equiv of ^{i}PrOH per zinc complex. Analytical analysis of the mixture confirmed the presence of 0.70 equiv of ^{i}PrOH. Anal. Calcd for $C_{12}H_{21}N_3S_2Cl_2O_8Zn \cdot 0.7{}^i$PrOH: C, 29.43; H, 4.66; N, 7.31. Found: C, 29.43; H, 4.74; N, 7.15.

X-ray Crystallography. A crystal of compounds **1**−**6**, **7·DMSO**, **8**, **9·2DMSO**, **11**, and **12** was mounted on a glass fiber with traces of viscous oil and then transferred to a Nonius KappaCCD diffractometer with Mo Kα radiation (λ = 0.71073 Å) for data collection at 200(1) K. For each compound, an initial set of cell constants was obtained from 10 frames of data that were collected with an oscillation range of 1 °/frame and an exposure time of 20 s/frame. Final cell constants for each complex were determined from a set a strong reflections from the actual data collection. For each data set, these reflections were indexed, integrated, and corrected for Lorentz, polarization, and absorption effects using DENZO-SMN, SCALEPAC, and Multiscan.[13] Each structure was solved by a combination of direct methods and heavy atom using SIR97. All of the non-hydrogen atoms were refined with anisotropic displacement coefficients. Unless otherwise noted, hydrogen atoms were assigned isotropic displacement coefficients U(H) = 1.2U(C) or 1.5U(Cmethyl), and their coordinates were allowed to ride on their respective carbons using SHELXL97.

Structure Solution and Refinement. In **1**, all hydrogen atoms were located and refined independently using SHELXL97. One perchlorate anion exhibited disorder. Each oxygen atom of this perchlorate (O(7)−O(10)) was split into two fragments (second fragment denoted by a prime) and refined. This refinement led to a 0.87:0.13 ratio in occupancy over two positions for each oxygen atom. In **2**, two formula units are present per asymmetric unit, with the second denoted by a prime. The methanol hydroxyl proton of the zinc-bound methanol for each formula unit was located and refined independently using SHELXL97. In **3**, the primary amine hydrogen atoms of the bmapa ligand were located and refined independently using SHELXL97. In **4**, the hydrogen atoms of the primary amine substituent of the bmapa ligand and the formamide hydrogen atom were located and refined independently using SHELXL97. In **5**, the position of one chlorine atom and an oxygen atom of a perchlorate anion were found to be disordered. Each was split into two fragments (second fragments denoted by a prime) and refined. This refinement led to a 0.77:0.23 ratio in occupancy over two positions for each atom. In **6**, all hydrogen atoms were located and refined independently, except those on C(14) which were assigned isotropic displacement coefficients. In **7·DMSO**, the hydrogen atoms of the primary amine substituent of the bmapa ligand were located and refined independently using SHELXL97. In **8**, two formula units are present in the asymmetric unit, with the second being denoted by an "A" designation. Each perchlorate anion present exhibited disorder. Each disordered atom was split into two fragments (second fragment denoted by a prime) and was refined. This refinement led to a 0.82:0.18 ratio in occupancy over two positions. For **9·2DMSO**, each DMSO ligand exhibited disorder in the position of the sulfur atom. Each disordered sulfur atom was split into two fragments (second fragment denoted by "A") and

(13) Otwinowski, Z.; Minor, W. *Methods Enzymol.* **1997**, *276*, 307−326.

Scheme 2. Synthesis of N/S-Ligated Zinc Alcohol Complexes

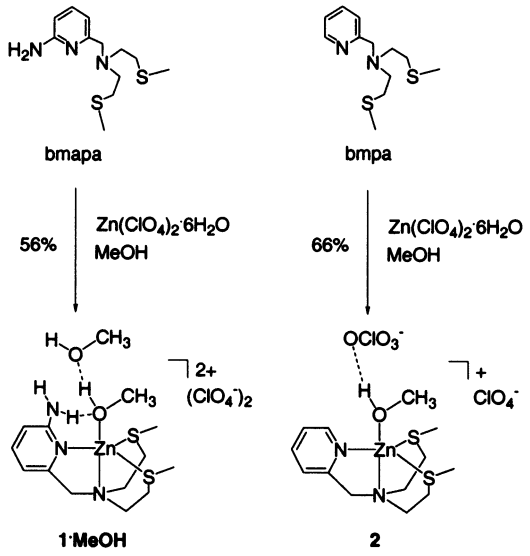

was refined. This refinement led to a 0.96:0.04 ratio for S3, a 0.92:0.08 ratio for S4, and a 0.62:0.38 ratio for S5. One perchlorate anion also exhibited disorder in the position of three oxygen atoms. Each disordered atom was split into two fragments (second fragment denoted by "A") and was refined. This refinement led to a 0.86:0.14 ratio in occupancy over two positions. In **11**, four formula units are present in the asymmetric unit, with the second, third, and fourth being denoted by "A", "B", and "C". In **12**, the hydrogen atoms of the primary amine substituent of the bmapa ligand were located and refined independently using SHELXL97.

Results

Synthesis and Isolation of Complexes. Alcohol Complexes. Treatment of a methanol solution of bmapa or bmpa with an equimolar amount of $Zn(ClO_4)_2 \cdot 6H_2O$ (Scheme 2) followed by crystallization from alcohol/ethyl ether solutions at ambient temperature yielded the crystalline methanol adducts $[(bmapa)Zn(MeOH)](ClO_4)_2$ (**1**)[14] and $[(bmpa)Zn(MeOH)](ClO_4)_2$ (**2**) in analytically pure form and in moderate yields (56−66%) after drying under vacuum.

Formamide Complexes. Addition of ∼1.5−2 equiv of *N*,*N*-dimethylformamide (DMF) or *N*-methylformamide (NMF) to an in situ generated methanol solution of **1** or **2** (Schemes 3 and 4) followed by precipitation using excess Et_2O yielded the formamide adducts $[(bmapa)Zn(DMF)](ClO_4)_2$ (**3**), $[(bmapa)Zn(NMF)](ClO_4)_2$ (**4**), and $[(bmpa)Zn(DMF)](ClO_4)_2$ (**5**). We note that ^{1}H NMR analyses of vacuum-dried samples of **5** recrystallized from ^{i}PrOH/MeOH/Et_2O always indicated the presence of a small amount of MeOH. Because this methanol cannot be removed under vacuum, this may indicate the presence of a small amount of $[(bmpa)Zn(MeOH)](ClO_4)_2$ (**2**) in bulk samples of **5**. While the *N*-methylformamide complex $[(bmpa)Zn(NMF)](ClO_4)_2$ (**6**) could be generated in and cleanly precipitated from methanol, attempts to obtain X-ray quality crystals from methanol-containing solutions always resulted in the isolation of **2**.

(14) Approximately one molecule of methanol is lost upon drying under vacuum, as indicated by elemental analysis of a bulk dried sample. The bulk sample is referred to herein as **1**.

Scheme 3. Synthesis of bmapa Zinc Formamide and Sulfoxide Complexes

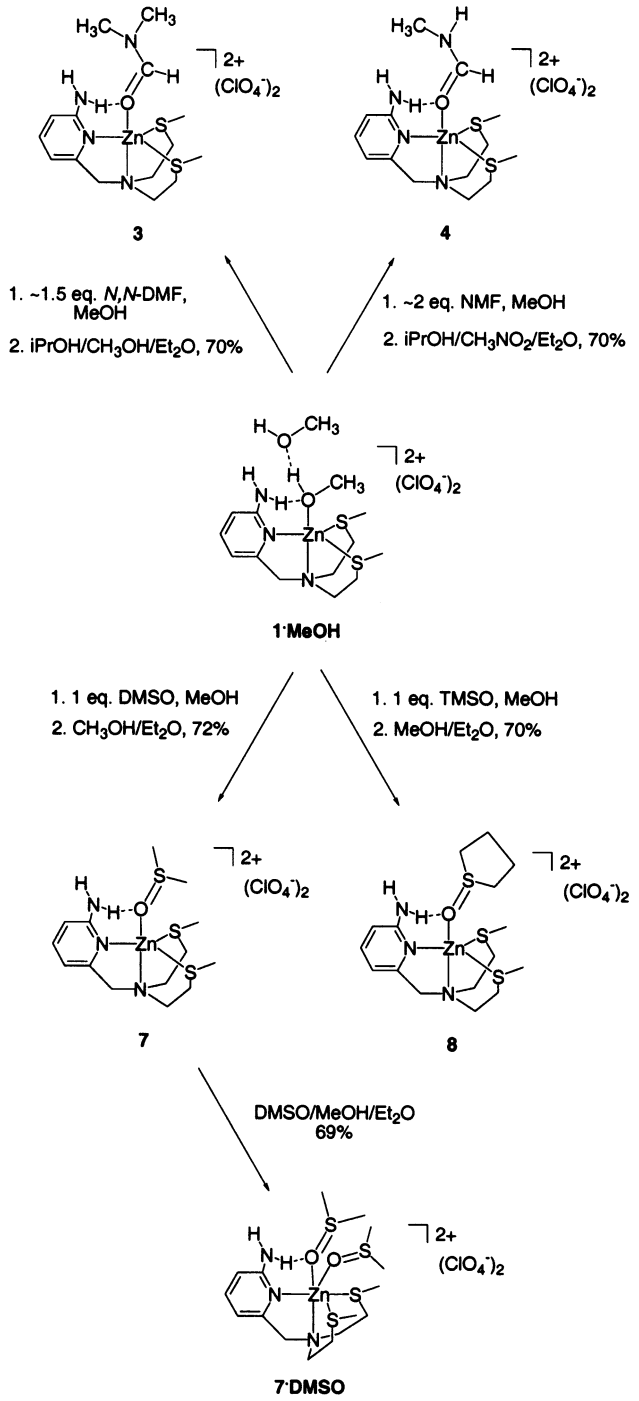

Therefore, to prepare analytically pure samples of **6**, the synthesis and recrystallization were conducted in similar fashion using CH_3NO_2-based solutions.

Sulfoxide Complexes. Addition of ∼1.0−1.5 equiv of dimethyl sulfoxide (DMSO) or tetramethylene sulfoxide (TMSO) to an in situ generated methanol solution of **1** or **2** followed by precipitation using excess Et_2O yielded the monosulfoxide adducts $[(bmapa)Zn(DMSO)](ClO_4)_2$ (**7**), $[(bmapa)Zn(TMSO)](ClO_4)_2$ (**8**), $[(bmpa)Zn(DMSO)](ClO_4)_2$ (**9**), and $[(bmpa)Zn(TMSO)](ClO_4)_2$ (**10**) as white powders (Schemes 3 and 4). Recrystallization of **8** from MeOH/Et_2O at ambient temperature yielded single crystals suitable for

Scheme 4. Synthesis of bmpa Zinc Formamide and Sulfoxide Complexes

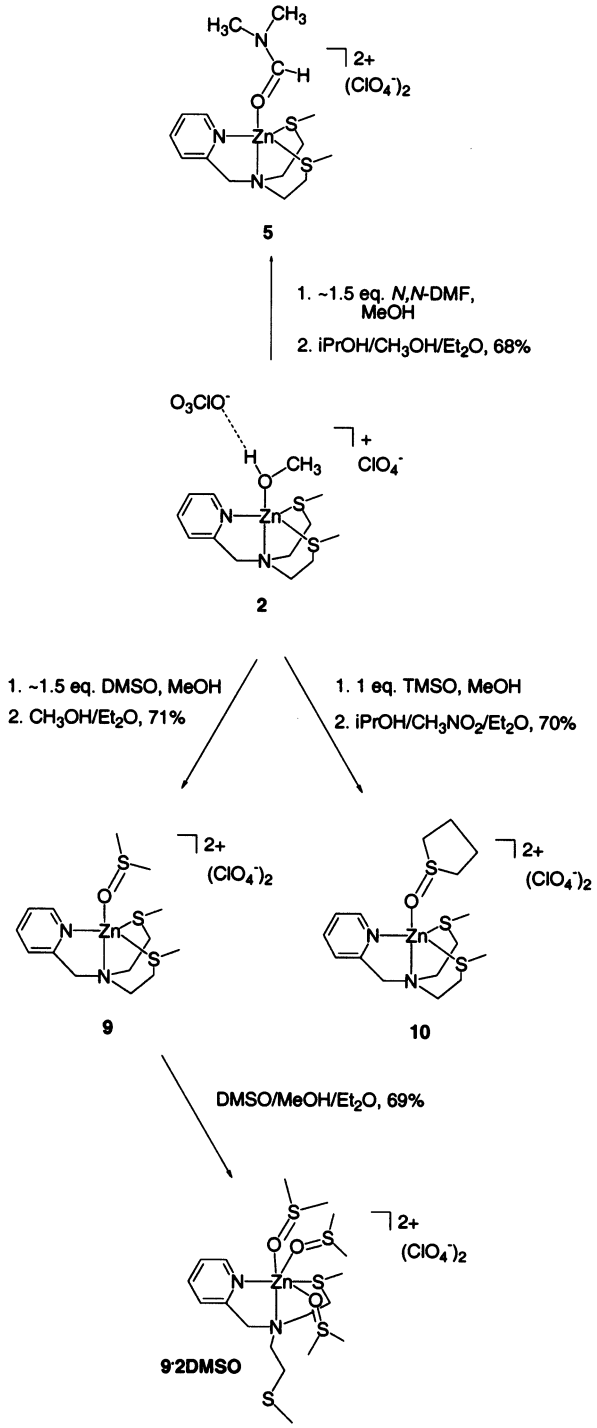

X-ray diffraction analysis. However, attempts to crystallize compounds **7**, **9**, and **10** from methanol solutions yielded only polycrystalline materials. Complexes **7** and **9** were recrystallized in the presence of excess DMSO. This led to the isolation and crystallographic characterization of [(bmapa)-$Zn(DMSO)_2](ClO_4)_2$ (**7·DMSO**) and [(bmpa)$Zn(DMSO)_3$]-$(ClO_4)_2$ (**9·2DMSO**).

Acetonitrile Complex. Solution spectroscopic studies of several bmapa derivatives (vida infra) suggested that, when acetonitrile is employed as a solvent, displacement of the neutral oxygen donor (e.g., DMF/NMF) from the zinc center may occur. To examine whether acetonitrile could potentially bind to the zinc center, the bmapa ligand was treated with $Zn(ClO_4)_2·6H_2O$ in CH_3CN (Scheme 5). The product was then precipitated by addition of Et_2O and recrystallized from ^{i}PrOH/CH_3CN/Et_2O to yield [(bmapa)$Zn(CH_3CN)](ClO_4)_2$ (**11**) as a crystalline solid suitable for X-ray crystallographic analysis. Drying of this crystalline product under vacuum results in partial loss of the CH_3CN ligand (as evidenced by characterization of the resulting solid by elemental analysis).

Scheme 5. Synthesis of Zinc Acetonitrile Complex

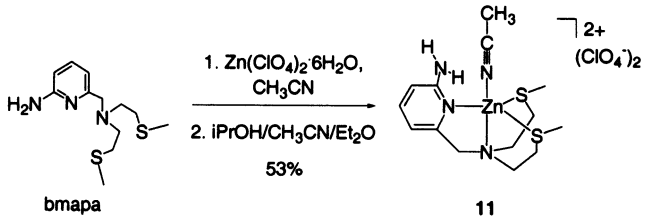

Scheme 6. Synthesis of Zinc Perchlorate Complex

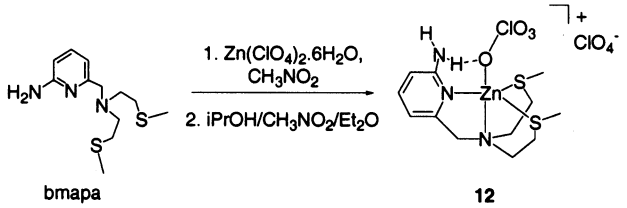

Perchlorate Complex. Solution spectroscopic studies of the zinc formamide complexes (**3**−**6**) in CH_3NO_2 solution (vida infra) also indicated displacement of the formamide donor (DMF/NMF) from the cationic zinc center. Because CH_3NO_2 is a poorly coordinating solvent and therefore probably does not directly compete with the neutral oxygen donor formamide molecule for coordination at the zinc center, we hypothesized that a perchlorate anion may, under these conditions, compete for a coordination position. To test this hypothesis, equimolar amounts of bmapa and $Zn(ClO_4)_2·6H_2O$ were stirred together in CH_3NO_2 (Scheme 6). Addition of excess Et_2O to this solution resulted in precipitation of a white solid. Recrystallization of the solid from ^{i}PrOH/CH_3NO_2/Et_2O at ambient temperature yielded an oil intermixed with small needle crystals with an analytical composition consistent with the formulation [(bmapa)Zn]-$(ClO_4)_2·0.7^i$PrOH. As outlined later, X-ray crystallographic analysis of a single-crystal derived from batches prepared by this method showed the presence of a mononuclear perchlorate-coordinated complex [(bmapa)$Zn(ClO_4)](ClO_4)$ (**12**) and no ^{i}PrOH solvate. However, on the basis of analytical analysis of the combined oil/crystalline sample, which indicated the presence of 0.7 equiv of ^{i}PrOH per complex, we suspect that the bulk isolated material is a mixture of two complexes, the perchlorate derivative [(bmapa)-$Zn(ClO_4)](ClO_4)$ (**12**) and a 2-propanol adduct (e.g., a possible formulation could be [(bmapa)Zn(^{i}PrOH)]$(ClO_4)_2$). Attempts to isolate pure **12** by changing the ^{i}PrOH/CH_3NO_2 ratio in the crystallization solution resulted only in varying amounts of the two products. Furthermore, attempts to prepare **12** from bmapa and $Zn(ClO_4)_2·6H_2O$ in CH_3NO_2 followed by crystallization from CH_3NO_2/Et_2O resulted only

Table 1. Summary of X-ray Crystallographic Data Collection and Refinement[a]

	1·MeOH	**2**	**3**	**4**	**5**	**6**
empirical formula	$C_{14}H_{29}N_3S_2$-$Cl_2O_{10}Zn$	$C_{13}H_{24}N_2S_2$-Cl_2O_9Zn	$C_{15}H_{28}N_4S_2$-Cl_2O_9Zn	$C_{14}H_{26}N_4S_2$-Cl_2O_9Zn	$C_{14}H_{26}N_3S_2$-Cl_2O_9Zn	$C_{14}H_{25}N_3S_2$-Cl_2O_9Zn
fw	599.79	552.73	608.80	594.78	593.79	579.76
cryst syst	monoclinic	monoclinic	triclinic	monoclinic	monoclinic	monoclinic
space group	$P2_1/n$	$P2_1/n$	$P\bar{1}$	$P2_1/n$	$P2_1/c$	$P2_1/c$
a (Å)	10.1319(3)	20.2104(6)	9.5182(3)	9.9083(2)	9.5672(2)	9.8436(2)
b (Å)	16.3454(4)	10.5822(2)	11.3430(3)	11.6725(2)	21.1583(4)	11.7100(3)
c (Å)	14.7150(2)	21.1025(6)	11.4818(2)	19.9993(5)	12.2516(2)	20.0699(2)
α (deg)			84.968(2)			
β (deg)	97.056(1)	101.624(1	87.343(2)	90.120(1)	104.278(1)	91.116(1)
γ (deg)			82.054(1)			
V (Å^3)	2418.4(1)	4420.6(2)	1222.3(1)	2313.0(1)	2403.4(1)	2313.0(1)
Z	4	8	2	4	4	4
d (calcd), Mg m^{-3}	1.647	1.661	1.654	1.708	1.641	1.665
temp (K)	200(1)	200(1)	200(1)	200(1)	200(1)	200(1)
cryst size (mm^3)	0.35 × 0.30 × 0.18	0.35 × 0.33 × 0.09	0.30 × 0.25 × 0.15	0.30 × 0.18 × 0.18	0.38 × 0.33 × 0.20	0.38 × 0.38 × 0.28
abs coeff (mm^{-1})	1.463	1.588	1.447	1.527	1.468	1.523
2θ max (deg)	65.14	60.12	60.08	54.88	55.00	55.02
refls collected	11992	20417	9256	9663	9320	9545
indep reflns	7215	12424	6887	5211	5422	5230
variable params	422	515	312	304	304	340
R1/wR2[b]	0.0363/0.0847	0.0522/0.1142	0.0376/0.0891	0.0307/0.0704	0.0363/0.0856	0.0397/0.0966
GOF (F^2)	1.025	1.028	1.029	1.015	1.038	1.021
largest diff (e$^-$ Å^{-3})	0.529/−0.438	0.621/−0.743	0.505/−0.521	0.412/−0.505	0.851/−0.573	0.690/−0.487

	7·DMSO	**8**	**9·(DMSO)$_2$**	**11**	**12**
empirical formula	$C_{16}H_{33}N_3S_4$-$Cl_2O_{10}Zn$	$C_{16}H_{29}N_3S_3$-Cl_2O_9Zn	$C_{18}H_{38}N_2S_5$-$Cl_2O_{11}Zn$	$C_{14}H_{24}N_4S_2$-Cl_2O_8Zn	$C_{12}H_{21}N_3S_2$-Cl_2O_8Zn
fw	691.96	639.87	755.07	576.76	535.71
cryst syst	monoclinic	monoclinic	monoclinic	orthorhombic	monoclinic
space group	Cc	$P2_1/n$	$P2/c$	$Pca2_1$	$P2_1/n$
a (Å)	10.6428(2)	19.0576(6)	12.2495(2)	22.6053(4)	8.0909(1)
b (Å)	19.2828(6)	11.8345(2)	10.5022(1)	11.1839(1)	14.1336(2)
c (Å)	14.0580(4)	23.7508(7)	24.4441(5)	36.7385(6)	18.0201(3)
α (deg)					
β (deg)	100.083(2)	104.522(1)	90.899(1)		95.4297
γ (deg)					
V (Å^3)	2840.4(1)	5185.5(2)	3144.2(1)	9288.1(2)	2051.4(1)
Z	4	8	4	16	4
d (calcd), Mg m^{-3}	1.618	1.639	1.595	1.650	1.735
temp (K)	200(1)	200(1)	200(1)	200(1)	200(1)
cryst size (mm^3)	0.33 × 0.25 × 0.10	0.23 × 0.15 × 0.13	0.30 × 0.25 × 0.23	0.30 × 0.25 × 0.15	0.30 × 0.25 × 0.20
abs coeff (mm^{-1})	1.399	1.445	1.336	1.515	1.706
2θ max (deg)	55.02	55.10	55.00	54.94	54.86
refls collected	5580	20751	12886	16781	8502
indep reflns	5579	11855	7144	16781	4644
variable params	340	670	387	1130	263
R1/wR2[b]	0.0341/0.0788	0.0689/0.1587	0.0394/0.0897	0.0502/0.0950	0.0302/0.0696
GOF (F^2)	1.058	1.016	1.026	1.039	1.041
largest diff (e$^-$ Å^{-3})	0.532/−0.471	0.746/−1.283	0.794/−0.780	0.652/−0.412	0.766/−0.657

[a] Radiation used: Mo Kα (λ = 0.71073 Å). Diffractometer used: Nonius KappaCCD. [b] $R1 = \sum||F_o| - |F_c||/\sum|F_o|$; $wR2 = [\sum[w(F_o^2 - F_c^2)^2]/[(F_o^2)^2]]^{1/2}$ where $w = 1/\sigma^2(F_o^2) + (aP)^2 + bP$.

in the isolation of an oily material that appears to contain water (as indicated by ^{1}H NMR).[15]

X-ray Crystallography. The X-ray crystal structures of [(bmapa)Zn(MeOH)](ClO$_4$)$_2$·MeOH (**1·MeOH**) and [(bmapa)Zn(DMF)](ClO$_4$)$_2$ (**3**) were reported previously; for reference, drawings of the cationic portions of these molecules are provided in Figures 3a and 4a. New X-ray crystallographic data for [(bmpa)Zn(MeOH)](ClO$_4$)$_2$ (**2**), [(bmapa)Zn(NMF)](ClO$_4$)$_2$ (**4**), [(bmpa)Zn(DMF)](ClO$_4$)$_2$ (**5**), [(bmpa)Zn(NMF)](ClO$_4$)$_2$ (**6**), [(bmapa)Zn(DMSO)$_2$]-(ClO$_4$)$_2$ (**7·DMSO**), [(bmapa)Zn(TMSO)](ClO$_4$)$_2$ (**8**), [(bmpa)-Zn(DMSO)$_3$](ClO$_4$)$_2$ (**9·2DMSO**), [(bmapa)Zn(CH$_3$CN)]-(ClO$_4$)$_2$ (**11**), and [(bmapa)Zn(ClO$_4$)](ClO$_4$) (**12**) are reported herein. Details of the data collection and refinement are given in Table 1. Selected bond distances and angles are given in Table 2.

A. Alcohol Complexes [(bmapa)Zn(MeOH)](ClO$_4$)$_2$·MeOH (1·MeOH) and [(bmpa)Zn(MeOH)](ClO$_4$)$_2$ (2). The structural features and metrical parameters for **1·MeOH** have been previously reported. Discussion of **1·MeOH** will therefore be limited to comparison of its structural features with those of the two structurally independent, but chemically similar formula units (designated as **2A** and **2B**) found in the asymmetric unit of **2**, and relevant literature compounds. Crystals of **2** suitable for X-ray diffraction analysis were grown from MeOH/^{i}PrOH/Et$_2$O. The five-coordinate zinc

(15) A broad peak at ∼2.7 ppm is present, which is suggestive of the presence of water.

Table 2. Selected Bond Lengths (Å) and Angles (deg) for Complexes Characterized by X-ray Crystallography[a]

[(bmapa)Zn(MeOH)](ClO$_4$)$_2$·MeOH (**1·MeOH**)

Zn(1)−O(1)	2.077(1)	Zn(1)−S(1)	2.434(1)
Zn(1)−N(2)	2.054(2)	Zn(1)−S(2)	2.452(1)
Zn(1)−N(3)	2.163(2)		
O(1)−Zn(1)−N(2)	100.97(6)	N(3)−Zn(1)−S(1)	86.58(5)
N(2)−Zn(1)−N(3)	80.76(6)	N(2)−Zn(1)−S(2)	137.55(5)
O(1)−Zn(1)−N(3)	176.55(6)	O(1)−Zn(1)−S(2)	91.55(4)
N(2)−Zn(1)−S(1)	109.92(5)	N(3)−Zn(1)−S(2)	85.19(4)
O(1)−Zn(1)−S(1)	95.57(5)	S(1)−Zn(1)−S(2)	108.95(2)

[(bmpa)Zn(MeOH)](ClO$_4$)$_2$ (**2**)

Cation 2A

Zn(1)−O(1)	2.078(2)	Zn(1)−S(1)	2.406(1)
Zn(1)−N(1)	2.040(3)	Zn(1)−S(2)	2.399(1)
Zn(1)−N(2)	2.184(3)		
O(1)−Zn(1)−N(1)	95.04(10)	N(2)−Zn(1)−S(1)	85.71(7)
N(1)−Zn(1)−N(2)	79.76(10)	N(1)−Zn(1)−S(2)	108.42(8)
O(1)−Zn(1)−N(2)	172.4(1)	O(1)−Zn(1)−S(2)	99.28(8)
N(1)−Zn(1)−S(1)	136.44(7)	N(2)−Zn(1)−S(2)	87.73(7)
O(1)−Zn(1)−S(1)	94.41(8)	S(1)−Zn(1)−S(2)	111.79(3)

Cation 2B

Zn(1′)−O(1′)	2.073(2)	Zn(1′)−S(1′)	2.415(1)
Zn(1′)−N(1′)	2.017(2)	Zn(1′)−S(2′)	2.366(1)
Zn(1′)−N(2′)	2.206(2)		
O(1′)−Zn(1′)−N(1′)	95.84(10)	N(2′)−Zn(1′)−S(1′)	85.77(7)
N(1′)−Zn(1′)−N(2′)	81.23(10)	N(1′)−Zn(1′)−S(2′)	130.69(8)
O(1′)−Zn(1′)−N(2′)	176.4(1)	O(1′)−Zn(1′)−S(2′)	96.80(8)
N(1′)−Zn(1′)−S(1′)	106.43(8)	N(2′)−Zn(1′)−S(2′)	86.70(7)
O(1′)−Zn(1′)−S(1′)	93.10(8)	S(1′)−Zn(1′)−S(2′)	120.18(4)

[(bmapa)Zn(DMF)](ClO$_4$)$_2$ (**3**)

Zn(1)−O(1)	2.049(2)	Zn(1)−S(1)	2.434(1)
Zn(1)−N(2)	2.054(2)	Zn(1)−S(2)	2.441(1)
Zn(1)−N(3)	2.189(2)		
O(1)−Zn(1)−N(2)	101.78(6)	N(3)−Zn(1)−S(1)	86.58(5)
N(2)−Zn(1)−N(3)	81.64(6)	N(2)−Zn(1)−S(2)	112.69(5)
O(1)−Zn(1)−N(3)	176.57(6)	O(1)−Zn(1)−S(2)	93.31(5)
N(2)−Zn(1)−S(1)	132.84(5)	N(3)−Zn(1)−S(2)	85.32(4)
O(1)−Zn(1)−S(1)	92.96(5)	S(1)−Zn(1)−S(2)	110.81(2)

[(bmapa)Zn(TMSO)](ClO$_4$)$_2$ (**8**)[b]

Zn(1)−O(1)	2.052(4)	Zn(1)−S(1)	2.448(2)
Zn(1)−N(2)	2.039(4)	Zn(1)−S(2)	2.432(2)
Zn(1)−N(3)	2.188(4)		
O(1)−Zn(1)−N(2)	101.11(2)	N(3)−Zn(1)−S(1)	84.37(13)
N(2)−Zn(1)−N(3)	80.88(16)	N(2)−Zn(1)−S(2)	139.11(1)
O(1)−Zn(1)−N(3)	176.07(2)	O(1)−Zn(1)−S(2)	94.70(12)
N(2)−Zn(1)−S(1)	106.22(1)	N(3)−Zn(1)−S(2)	84.52(12)
O(1)−Zn(1)−S(1)	92.30(14)	S(1)−Zn(1)−S(2)	110.07(6)

[(bmapa)Zn(CH$_3$CN)](ClO$_4$)$_2$ (**11**)[c]

Zn(1)−N(4)	2.123(5)	Zn(1)−S(1)	2.418(2)
Zn(1)−N(2)	2.047(5)	Zn(1)−S(2)	2.452(2)
Zn(1)−N(3)	2.204(4)		
N(4)−Zn(1)−N(2)	105.80(2)	N(3)−Zn(1)−S(1)	84.44(14)
N(2)−Zn(1)−N(3)	81.33(18)	N(2)−Zn(1)−S(2)	109.07(1)
N(4)−Zn(1)−N(3)	172.9(2)	N(4)−Zn(1)−S(2)	91.82(14)
N(2)−Zn(1)−S(1)	134.45(1)	N(3)−Zn(1)−S(2)	85.49(11)
N(4)−Zn(1)−S(1)	90.52(15)	S(1)−Zn(1)−S(2)	112.64(6)

[(bmapa)Zn(NMF)](ClO$_4$)$_2$ (**4**)

Zn(1)−O(1)	2.042(2)	Zn(1)−S(1)	2.445(1)
Zn(1)−N(2)	2.048(2)	Zn(1)−S(2)	2.425(1)
Zn(1)−N(3)	2.172(2)		
O(1)−Zn(1)−N(2)	101.05(6)	N(3)−Zn(1)−S(1)	84.88(4)
N(2)−Zn(1)−N(3)	81.69(6)	N(2)−Zn(1)−S(2)	133.00(5)
O(1)−Zn(1)−N(3)	173.76(6)	O(1)−Zn(1)−S(2)	96.69(4)
N(2)−Zn(1)−S(1)	115.93(5)	N(3)−Zn(1)−S(2)	85.28(5)
O(1)−Zn(1)−S(1)	88.89(5)	S(1)−Zn(1)−S(2)	107.52(2)

[(bmpa)Zn(DMF)](ClO$_4$)$_2$ (**5**)

Zn(1)−O(1)	2.022(2)	Zn(1)−S(1)	2.400(1)
Zn(1)−N(1)	2.044(2)	Zn(1)−S(2)	2.443(1)
Zn(1)−N(2)	2.193(2)		
O(1)−Zn(1)−N(1)	92.53(8)	N(2)−Zn(1)−S(1)	85.91(5)
N(1)−Zn(1)−N(2)	80.18(7)	N(1)−Zn(1)−S(2)	120.17(6)
O(1)−Zn(1)−N(2)	170.76(7)	O(1)−Zn(1)−S(2)	94.38(6)
N(1)−Zn(1)−S(1)	124.08(6)	N(2)−Zn(1)−S(2)	84.54(5)
O(1)−Zn(1)−S(1)	102.96(6)	S(1)−Zn(1)−S(2)	111.85(2)

[(bmpa)Zn(NMF)](ClO$_4$)$_2$ (**6**)

Zn(1)−O(1)	2.021(2)	Zn(1)−S(1)	2.399(1)
Zn(1)−N(1)	2.035(2)	Zn(1)−S(2)	2.439(1)
Zn(1)−N(2)	2.204(2)		
O(1)−Zn(1)−N(1)	95.51(9)	N(2)−Zn(1)−S(1)	86.20(6)
N(1)−Zn(1)−N(2)	80.42(6)	N(1)−Zn(1)−S(2)	116.86(7)
O(1)−Zn(1)−N(2)	170.97(8)	O(1)−Zn(1)−S(2)	89.72(7)
N(1)−Zn(1)−S(1)	130.50(7)	N(2)−Zn(1)−S(2)	85.02(6)
O(1)−Zn(1)−S(1)	102.48(6)	S(1)−Zn(1)−S(2)	109.03(3)

[(bmapa)Zn(DMSO)$_2$](ClO$_4$)$_2$ (**7·DMSO**)

Zn(1)−O(1)	2.053(2)	Zn(1)−N(3)	2.217(3)
Zn(1)−N(2)	2.070(3)	Zn(1)−S(1)	2.486(1)
Zn(1)−O(2)	2.183(2)	Zn(1)−S(2)	2.700(1)
O(1)−Zn(1)−N(2)	102.16(1)	O(2)−Zn(1)−S(2)	74.46(7)
O(1)−Zn(1)−O(2)	92.84(10)	N(3)−Zn(1)−S(2)	84.87(7)
N(2)−Zn(1)−O(2)	87.59(10)	O(1)−Zn(1)−S(1)	86.29(8)
O(1)−Zn(1)−N(3)	165.78(1)	N(2)−Zn(1)−S(1)	94.49(8)
N(2)−Zn(1)−N(3)	80.68(10)	O(2)−Zn(1)−S(1)	177.87(8)
O(2)−Zn(1)−N(3)	95.57(5)	N(3)−Zn(1)−S(1)	79.58(8)
O(1)−Zn(1)−S(2)	101.23(1)	S(1)−Zn(1)−S(2)	103.71(4)
N(2)−Zn(1)−S(2)	154.28(8)		

[(bmpa)Zn(DMSO)$_3$](ClO$_4$)$_2$ (**9·2DMSO**)

Zn(1)−O(1)	2.048(2)	Zn(1)−N(1)	2.147(2)
Zn(1)−O(2)	2.075(2)	Zn(1)−N(2)	2.257(2)
Zn(1)−O(3)	2.102(2)	Zn(1)−S(1)	2.636(1)
O(1)−Zn(1)−O(2)	93.30(8)	O(3)−Zn(1)−N(2)	94.30(7)
O(1)−Zn(1)−O(3)	91.50(8)	N(1)−Zn(1)−N(2)	78.76(7)
O(2)−Zn(1)−O(3)	98.79(8)	O(1)−Zn(1)−S(1)	84.79(5)
O(1)−Zn(1)−N(1)	171.16(7)	O(2)−Zn(1)−S(1)	92.99(6)
O(2)−Zn(1)−N(1)	91.65(8)	O(3)−Zn(1)−S(1)	175.48(6)
O(3)−Zn(1)−N(1)	95.84(8)	N(1)−Zn(1)−S(1)	87.65(6)
O(1)−Zn(1)−N(2)	95.81(7)	N(2)−Zn(1)−S(1)	83.54(5)
O(2)−Zn(1)−N(2)	169.90(8)		

[(bmpa)Zn(ClO$_4$)]ClO$_4$ (**12**)

Zn(1)−O(1)	2.183(2)	Zn(1)−S(1)	2.402(1)
Zn(1)−N(2)	2.154(2)	Zn(1)−S(2)	2.385(1)
Zn(1)−N(3)	2.041(2)		
O(1)−Zn(1)−N(2)	173.67(7)	N(3)−Zn(1)−S(1)	112.98(5)
N(2)−Zn(1)−N(3)	82.72(7)	N(2)−Zn(1)−S(2)	86.83(5)
O(1)−Zn(1)−N(3)	99.05(7)	O(1)−Zn(1)−S(2)	87.52(5)
N(2)−Zn(1)−S(1)	87.48(5)	N(3)−Zn(1)−S(2)	132.33(5)
O(1)−Zn(1)−S(1)	97.34(5)	S(1)−Zn(1)−S(2)	112.84(2)

[a] Estimated standard deviations indicated in parentheses. [b] Metrical parameters are given only for one of two independent cations in the asymmetric unit. [c] Metrical parameters are given only for one of four independent cations in the asymmetric unit.

ions in **2A**/**2B** exhibit a distorted trigonal bipyramidal geometry (**2A**: $\tau = 0.60$; **2B**: $\tau = 0.76$)[16] with the pyridyl nitrogen and sulfur donors in the equatorial plane (Figure 3b). The independent cations differ slightly in their respective Zn−S bond lengths (**2A**, Zn−S(1) 2.406(1), Zn−S(2) 2.399(1) Å; **2B**, Zn−S(1) 2.415(1), Zn−S(2) 2.366(1) Å) with the average Zn−S distances in **2A**/**2B** (2.40/2.39 Å) being slightly shorter than that observed for **1·MeOH** (Zn−S_{av} 2.44 Å). Differences between **2A**/**2B** are also found in the bond angles of the equatorial plane (S(1)−Zn−S(2) **2A**,

(16) Addison, A. W.; Rao, T. N.; Reedijk, J.; van Rijn, J.; Verschoor, G. C. *J. Chem. Soc., Dalton Trans.* **1984**, 1349−1356.

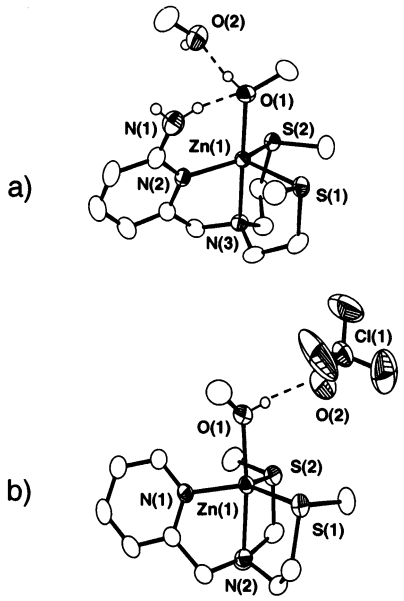

Figure 3. ORTEP representations of the cationic portions of (a) [(bmapa)Zn(MeOH)]$(ClO_4)_2$·MeOH (**1·MeOH**) and (b) [(bmpa)Zn(MeOH)]$(ClO_4)_2$ (**2**). Only one of two structurally distinct, but chemically similar, cations (**2A** and **2B**) found in the asymmetric unit of **2** is shown. All ellipsoids are drawn at the 35% probability level (all hydrogen atoms other than the primary amine and alcohol protons are omitted for clarity).

111.79(3)°, **2B**, 120.18(4)°; N(1)−Zn−S(1) **2A**, 136.44(7)°, **2B**, 106.43(8)°; N(1)−Zn−S(2) **2A**, 108.42(8)°, **2B**, 130.69(8)°) with the most notable feature being the smaller S(1)−Zn−S(2) angle in **2A**, a value similar to that found for the S(1)−Zn−S(2) angle in **1·MeOH** (108.95(2)°). In each independent cation of **2**, the methyl group of the zinc-bound alcohol is oriented toward the larger N(1)−Zn−S angle. The presence of the primary amine hydrogen bond donor moiety in the methanol complex **1·MeOH** enforces a different orientation of the alcohol alkyl group relative to the zinc-ligating atoms of the equatorial plane, with the methyl alcohol substituent in **1·MeOH** being oriented between the two zinc−sulfur bonds.

Mononuclear nitrogen/sulfur-ligated zinc alcohol complexes relevant to the substrate-bound form of liver alcohol dehydrogenase are rare.[3,4] The most structurally relevant compound reported to date in terms of modeling the exact NS_2 zinc coordination environment found in LADH is the mononuclear complex [HB(tim^{o-An})$_2$(pz^{Ph,Me})Zn(EtOH)]ClO_4.[3] In part because of the pentacoordinate nature of the zinc center found in **1·MeOH** and **2A/2B**, the Zn−O (Table 3) and Zn−S (**1·MeOH**, 2.434(1), 2.452(1) Å; **2A**, 2.406(1), 2.399(1) Å; **2B**, 2.415(1), 2.366(1) Å) distances in these complexes are elongated as compared to those found in [HB(tim^{o-An})$_2$(pz^{Ph,Me})Zn(EtOH)]ClO_4 (Zn−S, 2.282(1) and 2.314(1) Å), the tetrahedral S_3-ligated zinc complex [(Tm^{Mes})Zn(MeOH)]ClO_4 (Zn−S, 2.338(1) and 2.320(1) Å), and the calixarene N_3-ligated [Zn($X_6Me_3ImMe_3$)(EtOH)]$(ClO_4)_2$.[3,4,8] We note that direct comparison of the Zn−O and Zn−S distances found **1** and **2A**/**2B**, or other model systems, with those found in alcohol adducts of LADH, is limited because of the 2.1 Å resolution of the only alcohol-bound structure of LADH reported to date.[9]

Table 3. Zn−O(Alcohol) Bond Distances

alcohol complex	Zn−O (Å)
[(bmapa)Zn(MeOH)]$(ClO_4)_2$·MeOH (**1·MeOH**)	2.077(1)[a]
[(bmpa)Zn(MeOH)]$(ClO_4)_2$ (**2A**)	2.078(1)[a]
[(bmapa)Zn(MeOH)]$(ClO_4)_2$ (**2B**)	2.073(1)[a]
{[Tm^{Mes}]Zn(MeOH)}$^+$	1.993(3)[b]
[HB(tim^{o-An})$_2$(pzPh,Me)Zn(EtOH)](ClO_4)	1.970(3)[c]
[Zn($X_6Me_3ImMe_3$)(EtOH)]$(ClO_4)_2$	1.984(5)[d]
LADH-PFB (2.1 Å resolution)	2.0[e]

[a] This work. [b] Kimblin, C.; Bridgewater, B. M.; Churchill, D.; Parkin, G. *Chem. Commun.* **1999**, 2301. [c] Seebacher, J.; Shu, M.; Vahrenkamp, H. *Chem. Commun.* **2001**, 1026. [d] Sénèque, O.; Giorgi, M.; Reinaud, O. *Chem. Commun.* **2001**, 984. [e] PFB = 2,3,4,5,6-pentafluorobenzyl alcohol. Ramaswamy, S.; Eklund, H.; Plapp, B. V. *Biochemistry* **1994**, *33*, 5320.

Notable structural differences between **1·MeOH** and the two independent molecules of **2** reside in the nature of the hydrogen-bonding interactions involving the zinc-bound methanol molecule. Specifically, in **1·MeOH**, the oxygen atom of the methanol ligand accepts a hydrogen bond from the primary amine moiety of the bmapa ligand (N(1)···O(1) 2.92 Å, N(1)−H···O(1) 147°). In addition, the alcohol proton of the zinc-bound methanol molecule is involved in a tight hydrogen-bonding interaction with a second molecule of methanol (O(1)···O(2) 2.58 Å, O(1)−H(O1)···O(2) 169°) within the crystalline lattice. This type of short hydrogen-bonding interaction involving the zinc-bound methanol mimics the hydrogen bond network involving Ser_{48} in LADH ($O(Ser_{48})$···O(alcohol) 2.6 Å)[9] and has also been observed in the X-ray crystal structures of [(Tm^{Mes})Zn(MeOH)]-ClO_4·MeOH (O(MeOH)···O(Zn−HOMe) 2.58 Å) and [HB(tim^{o-An})$_2$(pz^{PhMe})Zn(EtOH)]ClO_4.[3,4] In **2A** and **2B**, the methanol proton participates in a hydrogen-bonding interaction involving a perchlorate anion (**2A**, O(1)···O(2) 2.83 Å, O(1)−H(O1)···O(2) 170°; **2B**, O(1)···O(2) 2.70 Å, O(1)−H(O1)···O(2) 175°). Comparison of the Zn−O bond distances in **1** and **2A**/**2B** (Table 3) indicates that a single hydrogen-bonding interaction (N···O, ∼2.92 Å), involving the zinc-bound methanol acting as a hydrogen bond acceptor, does not significantly influence Zn−O(alcohol) bonding.

B. Formamide Complexes [(bmapa)Zn(DMF)]$(ClO_4)_2$ (3), [(bmapa)Zn(NMF)]$(ClO_4)_2$ (4), [(bmpa)Zn(DMF)]-$(ClO_4)_2$ (5), and [(bmpa)Zn(NMF)]$(ClO_4)_2$ (6). The cationic portions of **3**−**6** are shown in Figure 4. Crystals of **3**−**5** suitable for X-ray diffraction analysis were grown from MeOH/^{i}PrOH/Et_2O. Attempts to grow single crystals of **6** under these conditions yielded exclusively [(bmpa)Zn-(MeOH)]$(ClO_4)_2$ (**2**). However, recrystallization of powdered samples of **6** from CH_3NO_2/^{i}PrOH/Et_2O yielded the desired complex as crystals suitable for X-ray diffraction analysis. All of the formamide derivatives possess a slightly distorted trigonal bipyramidal geometry (**3**, $\tau = 0.73$; **4**, $\tau = 0.68$; **5**, $\tau = 0.78$; **6**, $\tau = 0.67$).[16] Complexes **4** and **6** both exhibit a trans orientation of the bound *N*-methylformamide.

The Zn−O(1) distance for the bmapa derivative **3** is slightly elongated (∼0.025 Å) as compared to the Zn−O(1) distance found in **5**. This lengthening of the Zn−O bond is likely due to the presence of a single hydrogen-bonding interaction involving the zinc-bound formamide oxygen in **3**. Specifically, with the formamide oxygen acting as a

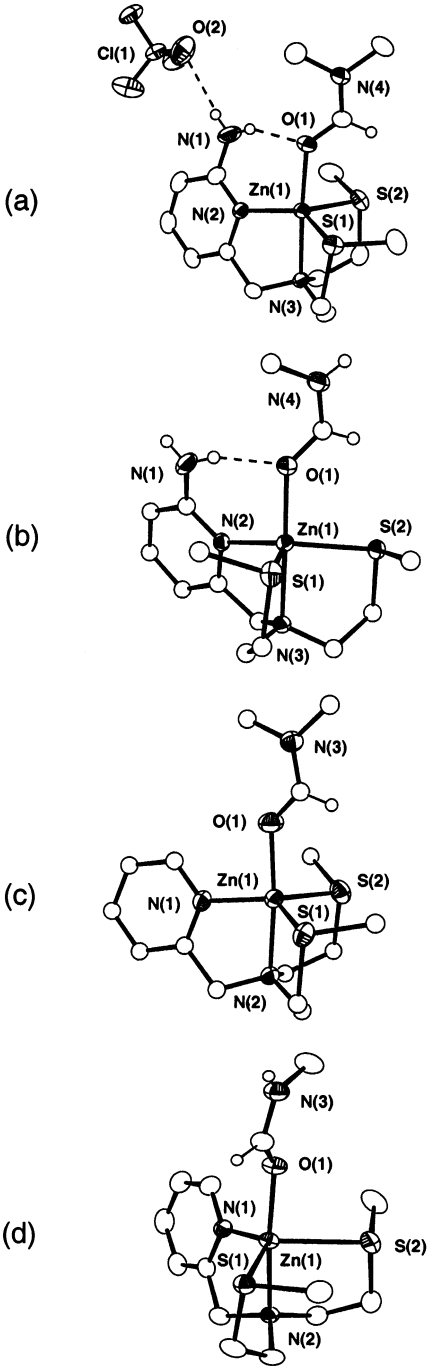

Figure 4. ORTEP representations of the cationic portions of (a) [(bmapa)Zn(DMF)]$(ClO_4)_2$ (**3**), (b) [(bmapa)Zn(NMF)]$(ClO_4)_2$ (**4**), (c) [(bmpa)Zn(DMF)]$(ClO_4)_2$ (**5**), and (d) [(bmpa)Zn(NMF)]$(ClO_4)_2$ (**6**). All ellipsoids are drawn at the 35% probability level (all hydrogen atoms other than the primary amine hydrogens and formamide hydrogens are omitted for clarity).

hydrogen bond acceptor, electron density would be removed from the formamide carbonyl unit, making it a weaker donor to the cationic zinc center. Notably, a similar change in Zn−O bond length ($\Delta \sim 0.02$ Å) is found in the *N*-methylformamide pair of complexes **4** and **6**. The Zn−O(formamide) bond distances in **3**−**6** are notably longer than that observed for formamide binding to a dicationic tetrahedral zinc ion encapsulated in a calixarene ligand (1.897(9) Å).[8] Finally, comparison of the Zn−O(formamide) distances in **3**−**6** with those found for formamide-inhibited forms of LADH offers little chemical insight because of the limited resolution (2.5 Å) of the reported X-ray crystal structures of the enzyme (Table 4).

Table 4. Zn−O(Formamide) and Zn−O(Sulfoxide) Bond Distances

formamide/sulfoxide complex	Zn−O (Å)
[(bmapa)Zn(DMF)]$(ClO_4)_2$ (**3**)	2.049(2)[a]
[(bmapa)Zn(NMF)]$(ClO_4)_2$ (**4**)	2.042(2)[a]
[(bmpa)Zn(DMF)]$(ClO_4)_2$ (**5**)	2.022(2)[a]
[(bmpa)Zn(NMF)]$(ClO_4)_2$ (**6**)	2.021(2)[a]
[Zn($X_6Et_3ImEt_3$)(NH_2CHO)]$(ClO_4)_2$	1.897(9)[b]
LADH-NCyForm (2.5 Å)	2.3[c]
LADH-NFormPip (2.5 Å)	2.3[c]
[(bmapa)Zn(TMSO)]$(ClO_4)_2$ (**8**)	2.052(4)[a]
[(bmapa)Zn(TMSO)]$(ClO_4)_2$ (**8A**)	2.018(5)[a]
LADH-(1S,3R)-BTO (2.1 Å)	2.2[d]
LADH-(1S,3S)-BTO (1.66 Å)	2.3[d]
LADH-DMSO (1.8 Å)	2.2[e]

[a] This work. [b] Sénèque, O.; Giorgi, M.; Reinaud, O. *Chem. Commun*. **2001**, 984. [c] NCyForm = *N*-cyclohexylformamide. NFormPip = *N*-formylpiperidine. Ramaswamy, S.; Scholze, M.; Plapp, B. V. *Biochemistry* **1997**, *36*, 3522. [d] BTO = 3-butythiolane 1-oxide. Cho, H.; Ramaswamy, S.; Plapp, B. V. *Biochemistry* **1997**, *36*, 382. [e] Al-Karadaghi, S.; Cedergren-Zeppezauer, E. S.; Hövmoller, S.; Petratos, K.; Terry, H.; Wilson, K. S. *Acta Crystallogr*. **1994**, *D50*, 793.

C. Sulfoxide Complexes [(bmapa)Zn(DMSO)$_2$]$(ClO_4)_2$ (7·DMSO), [(bmapa)Zn(TMSO)]$(ClO_4)_2$ (8), and [(bmpa)-Zn(DMSO)$_3$]$(ClO_4)_2$ (9·2DMSO). Mononuclear zinc complexes of the bmapa and bmpa ligands may be crystallized with one or more bound sulfoxide ligands depending upon the solvent conditions employed for crystallization. For example, recrystallization of analytically pure powders of **7**−**10** from CH_3NO_2/Et_2O (**7**, **9**, and **10**) or CH_3OH/Et_2O (**8**) yielded crystalline complexes of the general formula [(ligand)Zn(sulfoxide)]$(ClO_4)_2$, one of which (**8**) was suitable for X-ray crystallographic analysis (Figure 5b). Attempts to recrystallize **7** and **9** from $CH_3OH/DMSO/Et_2O$ resulted in the isolation of single crystals of [(bmapa)Zn$(DMSO)_2$]-$(ClO_4)_2$ (**7·DMSO**) and [(bmpa)Zn$(DMSO)_3$]$(ClO_4)_2$ (**9·2DMSO**) (Figure 5a,c). Two chemically similar, but structurally distinct, formula units are found within the asymmetric unit of **8**. Only the cationic portion of one of these formula units will be discussed herein. As shown in Figure 5b, the five-coordinate TMSO complex (**8**) is structurally similar to the formamide derivatives previously described. The zinc center again exhibits a distorted trigonal bipyramidal geometry ($\tau = 0.62$)[16] with the sulfoxide ligand occupying a coordination position trans to the tertiary nitrogen of the bmapa ligand. Notably, the Zn−O(sulfoxide) distance for **8** (2.052(4) Å; **8A**, 2.018(5) Å) is on the short end of the range possible for zinc-bound sulfoxide inhibitors in LADH, when the resolution of the protein structure is considered (Table 4). A hydrogen-bonding interaction between the primary amine of the bmapa ligand and the zinc-bound oxygen atom of the sulfoxide is indicated in the solid state structure by the short N(1)···O(1) (2.83(2) Å) heteroatom distance.

The complexes possessing more than one bound sulfoxide ligand, **7·DMSO** and **9·2DMSO**, both exhibit a pseudo-octahedral geometry. In **7·DMSO**, the thioether sulfur positioned trans to a bound sulfoxide ligand interacts only very weakly with the zinc center (Zn(1)···S(2) 2.700(1) Å).

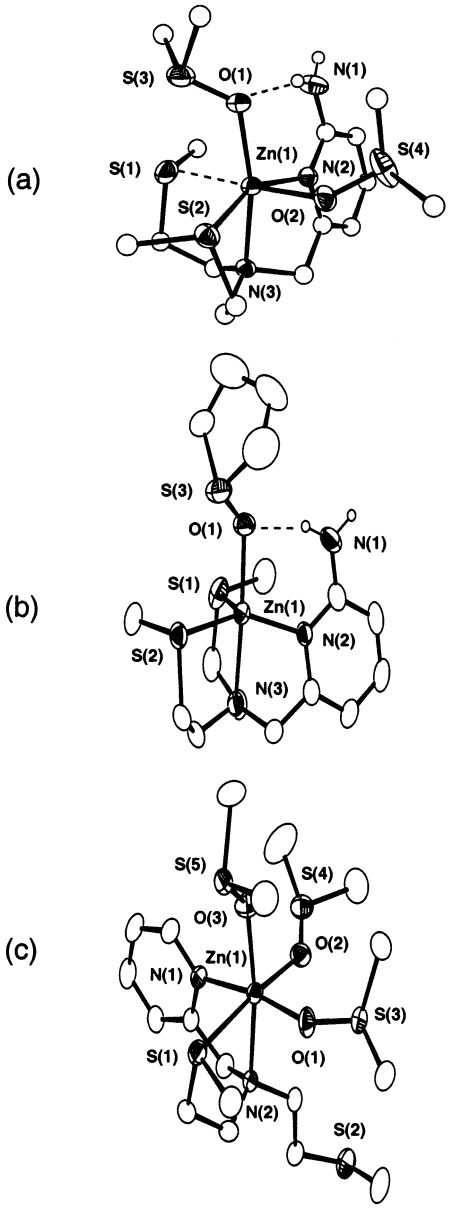

Figure 5. ORTEP representations of the cationic portions of (a) [(bmapa)-$Zn(DMSO)_2](ClO_4)_2$ (**7·DMSO**), (b) $[(bmapa)Zn(TMSO)](ClO_4)_2$ (**8**), and (c) $[(bmpa)Zn(DMSO)_3](ClO_4)_2$ (**9·2DMSO**). Only one of two structurally unique, but chemically similar, cations (**8** and **8A**) found in the asymmetric unit of **8** is shown. All ellipsoids are drawn at the 35% probability level (all hydrogen atoms except primary amine protons not shown for clarity).

The remaining zinc−thioether sulfur interaction (Zn(1)−S(1), 2.486(1) Å) is also slightly longer than the average Zn−S(thioether) distance found in **8** (2.44 Å). In **9·2DMSO**, one thioether sulfur (S(2)) is completely dissociated from the zinc center, whereas the second (S(1)) participates in a weak bonding interaction (Zn(1)−S(1), 2.636(1) Å) with the zinc ion. In **7·DMSO** and **9·2DMSO**, the Zn−O(sulfoxide) distances fall in the range 2.05−2.18 Å.

D. Acetonitrile Complex $[(bmapa)Zn(CH_3CN)](ClO_4)_2$ (11). Single crystals of $[(bmapa)Zn(CH_3CN)](ClO_4)_2$ (**11**) suitable for X-ray diffraction analysis were obtained from recrystallization of the powdered form of the complex from $^{i}PrOH/CH_3CN/Et_2O$. Similar to the alcohol- and formamide-bound complexes previously discussed, the cationic zinc center of **11** (Figure 6) exhibits a distorted trigonal bipyramidal geometry ($\tau = 0.64$)[16] with the acetonitrile ligand occupying the coordination position trans to the tertiary nitrogen of the ligand. Although no lone pair is available on the bound nitrile ligand to participate in a hydrogen-bonding interaction with the primary amine group of the bmapa ligand, the observed N(1)···N(4) heteroatom distance in **11** is still short (3.02 Å).

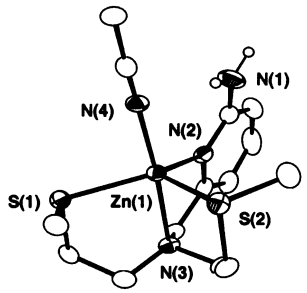

Figure 6. ORTEP representation of the cationic portion of $[(bmapa)Zn(CH_3CN)](ClO_4)_2$ (**11**). Only one of four structurally unique, but chemically similar, cations (**11**, **11A**, **11B**, and **11C**) found in the asymmetric unit of **11** is shown. All ellipsoids are drawn at the 35% probability level (all hydrogen atoms except primary amine protons not shown for clarity).

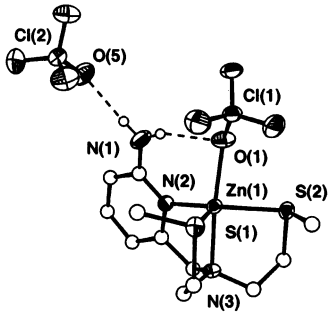

Figure 7. ORTEP representation of the X-ray structure of $[(bmapa)Zn(ClO_4)]ClO_4$ (**12**). All ellipsoids are drawn at the 35% probability level (all hydrogen atoms except primary amine protons not shown for clarity).

E. Perchlorate Complex $[(bmapa)Zn(ClO_4)](ClO_4)$ (12). Because solution spectroscopic studies (vida infra) of the formamide complexes were also conducted in CH_3NO_2, we have examined whether competition with perchlorate anion binding is feasible in CH_3NO_2 solution. As a portion of this work, we have isolated and crystallographically characterized the mononuclear zinc perchlorate complex $[(bmapa)Zn(ClO_4)]ClO_4$ (**12**). The distorted trigonal bipyramidal zinc center ($\tau = 0.69$)[16] found in **12** exhibits binding of a single perchlorate anion (Figure 7). The Zn−O(1) distance (2.183(2) Å) is similar to that found in $[(bmnpa)Zn(ClO_4)]ClO_4$ (2.174(3) Å).[17] An intramolecular hydrogen-bonding interaction is present between the zinc-bound oxygen atom of the perchlorate anion and the primary amine donor (O(1)···N(1) 2.89(1) Å, N(1)−H···O(1) 153(3)°).

Spectroscopic Properties. Solid State FTIR. Examination of the solid state FTIR properties of **1**−**12** (Table 5; Table S1 in the Supporting Information) has enabled identification of spectroscopic tags associated with hydrogen-bonding and neutral oxygen donor binding interactions within

(17) Berreau, L. M.; Allred, R. A.; Makowska-Grzyska, M. M.; Arif, A. M. *Chem. Commun.* **2000**, 1423−1424.

Table 5. Selected Solid State FTIR Data for bmapa and bmpa Zinc Complexes

	FTIR[a] (cm^{-1})				
complex	ν_{N-H}[b]	δ_{N-H}[c]	$\nu_{amide\ I}$	$\nu_{S=O}$	ν_{X-}[d]
1	3477, 3381[e]	1637			1114, 627
2					1094, 624
3	3444, 3357	1622	1663		1094, 625
4	3452, 3361	1637	1659		1093, 623
5			1663		1090, 624
6			1650		1093, 623
7	3449, 3353	1645		960[f]	1090, 623
7-d_6	3449, 3353	1645		968	1091, 623
8	3434, 3342	1649		947[g]	1093, 623
9				963[f]	1092, 624
10				965[g]	1091, 623
11[h]	3477, 3378	1638			1107, 624
12	3477, 3381	1637			1109, 625

[a] FTIR spectra of zinc complexes were collected as dilute KBr pellets. [b] Asymmetric and symmetric stretching vibrations associated with primary amine group of the bmapa ligand. [c] Bending vibrations associated with primary amine group of the bmapa ligand. [d] Vibrations of counterion. [e] Multiple broad bands associated with ν_{N-H} of amine and ν_{O-H} of methanol molecule. [f] This vibration may not simply be assumed to be $\nu_{S=O}$, as a $\rho_r(CH_3)$ vibration for DMSO is also present in the same region. Comparison of spectra of complexes generated from d_6-DMSO is necessary to confirm the assignment of the vibration as $\nu_{S=O}$.[18] [g] TMSO derivatives do not possess the $\rho_r(CH_3)$ vibration; therefore, $\nu_{S=O}$ may be directly assigned. [h] ν_{CN} was observed at 2272 cm^{-1}.

this family of complexes. In regard to hydrogen-bonding involving the bmapa supporting ligand, complexes **1**, **3**, **4**, **7**, **8**, **11**, and **12** each exhibit a pair of vibrations in the region 3500−3300 cm^{-1} which may be assigned as the asymmetric and symmetric stretching vibrations of the primary amine group. In **1** and **12**, this pair of vibrations is found at slightly higher energy, consistent with the fact that the average hydrogen bond heteroatom distance in these compounds ($N(1)\cdots O(1)_{av}$ > 3.0 Å) exceeds that found in the formamide (**3** and **4**) and sulfoxide (**8**) derivatives ($N(1)\cdots O(1)_{av}$ ∼ 2.85−2.97 Å). This indicates that the hydrogen-bonding interactions found in **1** and **12** are slightly weaker than those found in **3**, **4**, **7**, and **8**.

The formamide derivatives **3**−**6** each exhibit an amide I stretching vibration that is shifted to lower energy as compared to the respective free formamide (DMF (1677 cm^{-1}) or NMF (1689 cm^{-1})) when analyzed as a neat solution. This shift is consistent with a decrease in the electron density of the amide carbonyl unit resulting from coordination to the cationic zinc center. Notably, while DMF derivatives **3** and **5** both exhibit a shift to lower energy of 14 cm^{-1} in the carbonyl stretching vibration, the overall magnitude of the shifts observed for the NMF complexes is larger (**4**, 30 cm^{-1}; **6**, 39 cm^{-1}). Comparison of the $\nu_{C=O}$ vibrations of **3** and **5** (both 1663 cm^{-1}) seems to suggest that the presence of an internal hydrogen bond donor does not perturb electronic properties of the carbonyl moiety. However, the observation of a ∼9 cm^{-1} difference in $\nu_{C=O}$ between **4** (1659 cm^{-1}) and **6** (1650 cm^{-1}) is interesting. As stated previously, elongation of the Zn−O(carbonyl) bond by ∼0.02 Å is observed for both **3** and **4**, as compared to their analogues, **5** and **6**, which do not possess an internal hydrogen bond donor. As the presence of the internal hydrogen bond donor in **4** would be expected to remove electron density from the amide carbonyl unit, it is currently difficult to rationalize why **4** would exhibit a carbonyl stretching vibration at higher energy. This could be a consequence of the slight weakening of the Zn−O(1) interaction in **4** versus **6**. However, this interpretation is questionable because of the identical $\nu_{C=O}$ vibrations (1663 cm^{-1}) observed for the other pairwise comparable formamide complexes **3** and **5**. Careful analysis of the X-ray structures of **4** and **6** revealed that other than the observed difference in Zn−O(1) bond lengths, the bound *N*-methylformamide ligands in these complexes exhibit nearly identical metrical parameters, with one small difference being in the Zn(1)−O(1)−C(13) bond angle (**4**, 129.35(19)°; **6**, 132.33(14)°).

Table 6. Selected Acetonitrile Solution FTIR Data for bmapa and bmpa Zinc Formamide Complexes

	FTIR (cm^{-1})[a]			
complex	δ_{N-H}[b]	$\nu_{amide\ I\ (coord)}$	$\nu_{amide\ I\ (noncoord)}$	ν_{X-}[c]
3	1642	*d*	1677	1101, 625
4	1640	*d*	1688	1101, 625
5		1658	1676	1097, 625
6		1653	1688	1098, 625

[a] FTIR spectra of zinc complexes were collected as 100 mM solutions in CH_3CN. [b] Bending vibrations associated with primary amine group of the bmapa ligand. [c] Vibrations of counterion. [d] A distinct amide I band of the coordinated amide is not observed, presumably because of overlap with the δ_{N-H} band.

The $\nu_{S=O}$ for sulfoxide complexes **7**−**10** is found in the region ∼945−970 cm^{-1} [18] and has been identified by isotopic labeling for **7**. For the DMSO derivatives **7** and **9**, a slight decrease (∼3 cm^{-1}) in $\nu_{S=O}$ is observed when the hydrogen bond donor is present. However, for the TMSO complexes **8** and **10**, the decrease in $\nu_{S=O}$ is much more significant (∼18 cm^{-1}). Because we have thus far been unable to characterize **7**, **9**, and **10** by X-ray crystallography, these interesting perturbations, induced by the presence of an internal hydrogen bond donor, remain under investigation.

Solution FTIR. Solution FTIR spectra of the formamide derivatives **5** and **6** obtained in CH_3CN (∼100 mM) exhibit $\nu_{C=O}$ vibrations consistent with the presence of both free and bound formamide (Table 6). For the bmapa derivatives **3** and **4**, a vibration indicative of the presence of coordinated formamide could not be conclusively identified, perhaps because of overlap with the δ_{N-H} vibration of the primary amine group of the bmapa ligand. While the determination of the relative amounts of free versus bound formamide in these systems is currently underway using a peak fitting approach to analyze the solution FTIR data reported herein,[19] it is apparent that for complexes **3**−**6** at least 40−50% of the formamide present in CH_3CN solution exists as free formamide. On the basis of our complementary synthetic studies, which indicate that acetonitrile binding can occur

(18) $\nu_{S=O}$ for oxygen-ligated DMSO complexes is typically found in the region ∼900−1000 cm^{-1}. Nakamoto, K. *Infrared and Raman Spectra of Inorganic and Coordination Compounds*, 5th ed.; Wiley-Interscience: New York, 1997.

(19) Determination of the exact amount of free vs bound formamide in **3**−**6** is complicated by the presence of ligand-based vibrations in the region 1600−1700 cm^{-1}. Deconvolution of these spectra using peak fitting software is currently in progress and will be reported in due course.

Table 7. Selected Nitromethane Solution FTIR Data for bmapa and bmpa Zinc Formamide Complexes

	FTIR (cm^{-1})[a]			
complex	δ_{N-H}[b]	$\nu_{amide\ I\ (coord)}$	$\nu_{amide\ I\ (noncoord)}$	ν_{X-}[c]
3	*d*	1667	*e*	1094, 625
4	1648	1661	1688	1094, 625
5		1659	*e*	1094, 625
6		1654	1684	1094, 625

[a] FTIR spectra of zinc complexes were collected as 100 mM solutions in CH_3NO_2. [b] Bending vibrations associated with primary amine group of the bmapa ligand. [c] Vibrations of counterion. [d] A distinct δ_{N-H} band is not observed, presumably because of overlap with the amide I band of the coordinated amide. [e] A distinct amide I band of the noncoordinated amide is not observed, presumably because of overlap with the amide I band of the coordinated amide.

to a bmapa-ligated zinc center (see complex **11**), we hypothesize that the formamide ligand of **3**−**6** is at least partially displaced in CH_3CN solution (eq 1) and that an acetonitrile adduct complex likely forms (e.g., [(bmapa)Zn(CH_3CN)](ClO_4)$_2$ (**11**)). We note that solution FTIR studies of the methanol complexes **1** and **2** and the sulfoxide-bound species **7**−**10** in CH_3CN were less informative, as diagnostic vibrations of the bound neutral oxygen donors, or the vibrations indicative of free alcohol or sulfoxide were not easily identified. For example, the $\nu_{S=O}$ vibration of free DMSO and TMSO is located beneath the strong asymmetric ν_{Cl-O} vibration of ClO_4^- at ∼1100 cm^{-1}, thus making it impossible by FTIR, with the present set of compounds, to determine whether the sulfoxide ligand of **7**, **8**, **9**, or **10** is released from the cationic zinc center in CH_3CN solution.

$$[LZn(formamide)](ClO_4)_2 + CH_3CN \underset{L = bmapa\ or\ bmpa}{\rightleftharpoons} [LZn(CH_3CN)](ClO_4)_2 + formamide \quad (1)$$

We have also examined the solution FTIR spectroscopic properties of the *N*,*N*-dimethylformamide adduct **3** in dry MeOH.[20] Under these conditions, the complex exhibits a single broad feature in the region 1600−1700 cm^{-1} and centered at ∼1660 cm^{-1}. Although this is near the position of the bound formamide $\nu_{C=O}$ in solid state spectra of **3** (1663 cm^{-1}), it is not possible to conclusively say from this experiment whether any free formamide is present in methanol solutions of **3**. The NMF derivative **4** exhibits poor solubility in methanol and, therefore, was not examined by solution FTIR in methanol. The bmpa formamide complexes **5** and **6** also exhibit a broad feature centered at 1668 and 1676 cm^{-1}, respectively. In both cases, this result is inconclusive regarding whether both free and bound formamide molecules are present in methanol solution.

In CH_3NO_2 solution at ambient temperature, FTIR spectra of **4** and **6** are again consistent with a mixture of free and bound formamide being present (Table 7). As the CH_3NO_2 solvent is unlikely to serve as a ligand for the cationic zinc center, we hypothesize that in this case the perchlorate anion may compete with formamide for a coordination position (eq 2). This hypothesis is supported by our results showing that the perchlorate derivative [(bmapa)Zn(ClO_4)]ClO_4 (**12**) may be isolated from CH_3NO_2 solution (vida supra).

$$[LZn(formamide)](ClO_4)_2 \underset{L = bmapa\ or\ bmpa}{\rightleftharpoons} [LZn(ClO_4)]ClO_4 + formamide \quad (2)$$

NMR Spectroscopy. We have also characterized the solution properties of the N/S-ligated zinc alcohol, formamide, and sulfoxide complexes reported herein using ^1H and ^{13}C NMR spectroscopy (Tables S2 and S3, Supporting Information). In CD_3CN solution, at ambient temperature, no significant change in chemical shift (^1H NMR < 0.08 ppm; ^{13}C < 0.4 ppm) is observed for the ^1H or ^{13}C resonances derived from the aromatic, benzylic, or SMe hydrogens of the supporting bmapa or bmpa ligands, as a result of change in the type of the exogenous donor ligand present (alcohol, formamide, or sulfoxide). This observation suggests a general similarity of overall structure of complexes **1**−**10** in CD_3CN solution. However, one notable difference between the complexes is variability in the chemical shift position of the bmapa NH_2 resonance depending on the nature of the neutral oxygen donor ligand present.[21] For example, in dry CD_3CN solution spectra of [(bmapa)Zn(CH_3OH)](ClO_4)$_2$ (**1**), the NH_2 resonance is found at 5.89 ppm, whereas, for the formamide derivatives [(bmapa)Zn(DMF)](ClO_4)$_2$ (**3**) and [(bmapa)Zn(NMF)](ClO_4)$_2$ (**4**), this resonance is found at 6.11 and 6.09 ppm, respectively. In the sulfoxide derivatives [(bmapa)Zn(DMSO)](ClO_4)$_2$ (**7**) and [(bmapa)Zn(TMSO)](ClO_4)$_2$ (**8**), this resonance is shifted even further downfield, appearing at 6.20 and 6.16 ppm, respectively. We note that the NH_2 chemical shifts observed for [(bmapa)Zn(CH_3CN)](ClO_4)$_2$ (**11**, 5.87 ppm) and [(bmapa)Zn(ClO_4)](ClO_4) (**12**, 5.88 ppm) in dry CD_3CN are very similar to the chemical shift observed for [(bmapa)Zn(CH_3OH)](ClO_4)$_2$ (**1**).

The formamide derivatives **3**−**6** each exhibit only one set of resonances for the exogenous oxygen donor ligand present. This indicates that, if free and zinc-bound formamides are present (as is suggested by the CH_3CN solution FTIR studies of **5** and **6**), they are in rapid exchange on the NMR time scale at ambient temperature. Cooling of a CD_3CN solution of **3** to ∼−40 °C did not induce peak broadening in the formamide ^1H NMR resonances, indicating that the exchange process for this complex remains rapid even at lower temperatures. Experimental attempts to measure the relative amounts of free versus bound formamide in **3**−**6** are currently in progress using both solution NMR (attempts at a binding constant determination) and FTIR methods. We note that only a single set of neutral oxygen donor ligand resonances are also observed in dry CD_3CN ^1H NMR spectra of the alcohol complexes **1** and **2** and the sulfoxide complexes **7**−**10**.

(20) This sample was run at a concentration < 100 mM because of limited solubility of **3** in MeOH.

(21) We have conducted a series of control experiments wherein to a dry CD_3CN solution of the bmapa ligand (0.02 M) was added a single equivalent of DMF, NMF, DMSO, or TMSO. No significant change (all < 0.007 ppm) in the chemical shift position of the NH_2 proton resonance of the bmapa ligand was observed for any of these control systems. This indicates that the deshielding of the NH_2 resonance observed in dry CD_3CN solution ^1H NMR spectra of **3**, **4**, **7**, and **8** is likely due to hydrogen-bonding involving the zinc-coordinated neutral oxygen donor ligand.

One final set of observations from the CD_3CN solution ^1H NMR spectra of complexes **1**−**12** concerns the chemical shift position of the resonances of the neutral oxygen donor ligands at ambient temperature. In **1**, the C*H*$_3$ resonance (singlet) for the methanol donor molecule is found at 3.30 ppm, very similar to what is observed for free methanol (3.27 ppm) under identical conditions. A resonance for the hydroxyl proton is not observed. For **2**, the C*H*$_3$ resonance is found at 3.27 ppm and is observed as a doublet. This doublet is coupled to a quartet at 2.36 ppm, which integrates to one proton, and may be assigned as the alcohol hydroxyl proton. Observation of this coupling indicates that the hydroxyl proton is in slow exchange on the NMR time scale in **2** in dry CD_3CN solution. The lack of resolution of a signal for the hydroxyl proton of methanol in dry CD_3CN solution ^1H NMR spectra of **1** is likely due to exchange of the methanol hydroxyl proton with the amine protons of the bmapa ligand. For the formamide complexes **3** and **4**, the N−C*H*$_3$ resonances are observed at 3.10/2.94 ppm (free DMF 2.88/2.78 ppm) and 2.83 ppm (free NMF, 2.67 ppm), respectively. The same resonances for the bmpa analogues **5** and **6** are found at 2.98/2.86 and 2.77 ppm, respectively. For the dimethyl sulfoxide derivative **7**, the methyl proton resonance of the sulfoxide ligand is shifted downfield in the complex relative to its position in free DMSO under identical conditions (**7**, 2.84 ppm; free DMSO, 2.50 ppm). For the bmpa analogue complex **9**, a slightly smaller downfield shift in the C*H*$_3$ resonance is observed (**9**, 2.75 ppm).

From the ^1H NMR data, the following conclusions can be made. First, the downfield shift of greatest magnitude for the bmapa N*H*$_2$ resonance is observed for sulfoxide complexes **7** and **8**, whereas the smallest downfield shift in the N*H*$_2$ resonance is observed for alcohol derivative **1**. Second, the largest downfield shift in the neutral oxygen donor ^1H NMR resonances is exhibited by the sulfoxide derivatives (**7**−**10**), whereas the smallest magnitude change in chemical shift for the donor protons is observed for the alcohol complexes **1** and **2**. Third, the ^1H NMR chemical shifts of the neutral oxygen donor hydrogens in the bmpa systems are deshielded to a lesser degree than are the corresponding resonances in the bmapa derivatives. These combined results show that the synthetic complexes outlined herein exhibit perturbations in solution spectroscopic features as a result of chemical perturbations in the (1) nature of the neutral oxygen donor ligand present and (2) the secondary interactions surrounding the N/S-ligated zinc ion.

Discussion

The preparation of synthetic complexes relevant to active site structures found in zinc enzymes has been an active area of research in the bioinorganic community for more than a decade.[22] However, despite these efforts, synthetic complexes relevant to proposed zinc species possessing a single neutral oxygen donor ligand (e.g., water, alcohol, aldehyde, ketone, amide, sulfoxide) have remained scarce,[8,23] despite the fact that such species are proposed to occur in resting state and substrate- and inhibitor-bound forms of various zinc enzymes. As an approach toward examining the chemistry of neutral oxygen donor complexes relevant to substrate- and inhibitor-bound forms of LADH, we have described herein our construction of a family of N/S-ligated zinc alcohol, formamide, and sulfoxide complexes. We have prepared these complexes using two N_2S_2 ligands that differ only in the presence of a single internal hydrogen bond donor. Therefore, while these ligands do not exactly mimic the dianionic NS_2 coordination environment of the zinc center in LADH, they do enable studies directed toward understanding how a single internal hydrogen bond donor, akin to Ser_{48} in the active site of the LADH, will influence neutral oxygen donor binding.

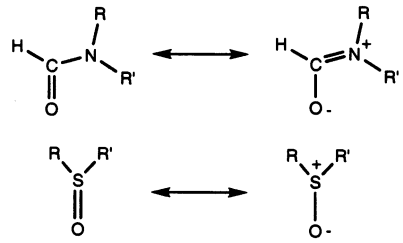

Figure 8. Resonance structures of formamides and sulfoxides.

In the work outlined herein, we have demonstrated that the presence of 1−2 equiv of a formamide or sulfoxide *in alcohol solutions* of our N/S-ligated zinc complexes resulted in the clean isolation of zinc complexes possessing a single bound formamide or sulfoxide ligand (complexes **3**−**5** and **7**−**10**). While preparation of two of the bmpa derivatives of this family (**6** and **10**) required the use of nonalcohol solvent systems in order to obtain clean crystalline samples for X-ray crystallography, the results indicate that the binding of a single formamide or sulfoxide ligand is at least competitive for a N/S-ligated zinc center in alcohol solution. This behavior may explain, in part, the observation that formamide and sulfoxide inhibitors of LADH are effective even in the presence of saturating amounts of alcohol.[5−7] A chemical rationale for the binding of formamide and sulfoxide derivatives to the cationic zinc center in alcohol solution resides in the fact that formamides and sulfoxides may form resonance structures wherein negative charge is located at the oxygen atom, making these species better donors for the cationic zinc center (Figure 8). A more quantitative way of discussing the relative Lewis basicity of various neutral oxygen donor species is in terms of a donor number (DN).[24] This parameter is defined as the negative enthalpy associated with the formation of a 1:1 adduct between antimony pentachloride and the electron pair donor in dilute solution, typically in the noncoordinating solvent 1,2-dichloroethane ($DN = -\Delta H_{D-SbCl_5}$/(kcal mol^{-1})). The larger donor numbers for dimethyl sulfoxide, *N*-methylformamide, and *N*,*N*-dimethylformamide, versus that determined for methanol, provides an indication that formamides and sulfoxides should

(22) See for example: Parkin, G. *Chem. Commun.* **2000**, 1971−1985.

(23) (a) Sénèque, O.; Rager, M.-N.; Giorgi, M.; Reinaud, O. *J. Am. Chem. Soc.* **2000**, *122*, 6183−6189. (b) Bergquist, C.; Parkin, G. *J. Am. Chem. Soc.* **1999**, *121*, 6322−6323.

(24) Gutmann, V. *The Donor*−*Acceptor Approach to Molecular Interactions*; Plenum: New York, 1978.

Table 8. Donor Numbers (DN) for Solvents

solvent	DN
acetonitrile	14.1[a]
methanol	19[b]
N-methylformamide	25[c]
N,*N*-dimethylformamide	26.6[a]
dimethyl sulfoxide	29.8[a]

[a] Gutmann, V. *The Donor−Acceptor Approach to Molecular Interactions*; Plenum: New York, 1978. [b] Determined by ^{23}Na NMR chemical shift of $NaClO_4$ in CH_3OH solution. Erlich, R. H.; Popov, A. I. *J. Am. Chem. Soc.* **1971**, *93*, 5620. [c] Chuang, H.; Soong, L. L.; Leroi, G. E.; Popov, A. I. *J. Solution Chem.* **1989**, *18*, 759.

form a stronger bonding interaction with the cationic zinc ion (Table 8).

Crystallographic characterization of the bmapa-ligated zinc complexes possessing a single bound alcohol (**1**), formamide (**3** and **4**), or sulfoxide (**8**) ligand has revealed that the Zn−O bond lengths observed in the synthetic complexes are similar, or perhaps slightly shorter, than those found in structurally characterized forms of LADH. For example, the Zn−O bond length found in alcohol adduct **1** (2.077(1) Å) is generally similar to that found in the pentafluorobenzyl alcohol adduct of LADH (2.0 Å). However, for the formamide (**3** and **4**) and sulfoxide (**8**) adducts, the Zn−O bond lengths (∼2.0 Å) are on the short end of the range (2.2−2.3 Å; resolution of structures 1.66−2.5 Å) possible for the enzyme. The observation of Zn−O distances in **1**, **3**, **4**, and **8**, which are similar or shorter than those found for the enzyme, is probably due to a number of factors, including the difference in Lewis acidity of the zinc center in the synthetic systems versus the active site zinc ion in LADH. Specifically, whereas in the synthetic systems described herein neutral thioether sulfur donors are present, in the enzyme the zinc cation is ligated by two anionic thiolate ligands. Taking this into account, the Zn−O distances observed for the synthetic formamide and sulfoxide derivatives probably reflect the greater cationic character of the zinc ion in the synthetic system.

The crystallographically characterized bmpa zinc alcohol (**2**) and formamide (**5** and **6**) complexes, which lack an internal hydrogen bond donor, follow the same general trend regarding Zn−O distances versus LADH ($d_{Zn-O(alcohol)} \approx d_{Zn-O(LADH-alcohol)}$, $d_{Zn-O(formamide)} \leq d_{Zn-O(LADH-formamide)}$) as those exhibited by the bmapa derivatives. However, direct comparison of the Zn−O distances of the bmpa compounds with those supported by the bmapa ligand does reveal interesting structural perturbations resulting from the presence of a single internal hydrogen bond donor. For example, whereas in $[(bmpa)Zn(MeOH)](ClO_4)_2$ (**2**), where the two independent cations within the asymmetric unit exhibit Zn−O bond lengths (2.078(1), 2.073(1) Å) identical to that observed for **1·MeOH** (2.077(1) Å), for the formamide adducts **5** and **6**, the observed Zn−O bond lengths are contracted slightly (∼0.02 Å) from those observed for **3** and **4**. For the formamide complexes, the elongation of the Zn−O bond in **3** and **4** is consistent with the notion that the hydrogen-bonding interaction will withdraw electron density from the formamide carbonyl units, weakening the overall bonding interaction with the cationic zinc center. However, a contributing factor to the elongation in the Zn−O(1) bond in **3** and **4**, as compared to that found for **5** and **6**, may also be a slightly increased Lewis basicity for the pyridyl donor of the bmapa ligand. Review of the relative basicity of pyridine ($pK_a = 5.14$) versus 2-aminopyridine ($pK_a = 6.71$)[25] indicates that the presence of the *o*-NH_2 group increases the basicity of the pyridyl nitrogen, thus making it a better donor to the zinc cation. Therefore, the elongation of the Zn−O(1) bond in bmapa derivatives **3** and **4** may be due to a combination of the presence of the hydrogen bond donor, which removes electron density from the formamide oxygen, and a slightly decreased Lewis acidity for the zinc center. Finally, we cannot rule out that a steric influence from the 2-amino group of the bmapa ligand may be at least in part responsible for the elongation of the Zn−O(1) bond in **3** and **4**. So why does the alcohol adduct **1·MeOH** not exhibit an elongation of the Zn−O bond as compared to **2**? This question is difficult to answer but may relate to differences in the nature of the hydrogen-bonding interactions found in **1·MeOH**, versus those of the formamide adducts **3** and **4**. As shown in Table 9, the hydrogen-bonding interaction involving the ligand primary amine group in **1·MeOH** is characterized by a slightly longer heteroatom distance and more acute ∠DHA than the corresponding parameters in **3** and **4**. While these differences are subtle, they do reflect the fact that the hydrogen-bonding interaction involving the zinc-bound alcohol in **1·MeOH** is weaker than the secondary interactions involving the zinc-bound formamides in **3** and **4**. Hence, the perturbation in Zn−O distance upon removal of the hydrogen

Table 9. Hydrogen-Bonding Interactions Involving Primary Amine Moiety in bmapa Zinc Complexes

	hydrogen bonds distances (Å) and angles (deg)			FTIR
no.	D−H···A	*d*(D···A)	∠DHA	ν_{N-H}[a]
1	$N(1)-H(1A)\cdots O(1)_{(MeOH)}$	2.92(1)	147	3477 3381
3	$N(1)-H(1A)\cdots O(1)_{(DMF)}$	2.86(1)	156	3444 3357
4	$N(1)-H(1A)\cdots O(1)_{(NMF)}$	2.85(1)	158	3452 3361
	$O_{(Ser48)}-H\cdots O_{(NCyForm)}$[b]	2.6		
	$O_{(Ser48)}-H\cdots O_{(NFormPip)}$[b]	2.5		
8[c]	$N(1)-H(1A)\cdots O(1)_{(TMSO)}$	2.83(2)	161	3434 3342
8A	$N(1A)-H(1A1)\cdots O(1A)_{(TMSO)}$	2.82(2)	157	
	$O_{(Ser48)}-H\cdots O_{(1S,3R)-BTO}$[d]	2.6		
	$O_{(Ser48)}-H\cdots O_{(1S,3S)-BTO}$[d]	2.6		
	$O_{(Ser48)}-H\cdots O_{DMSO}$[e]	2.6		
12	$N(1)-H(1A)\cdots O(1)(ClO_4)$[f]	2.89(1)	153	3477 3381
	$N(1)-H(1B)\cdots O(5)(ClO_4)$	3.14(1)	170	

[a] Asymmetric and symmetric stretching vibrations of primary amine group of bmapa ligand. [b] NCyForm = *N*-cyclohexylformamide. NFormPip = *N*-formylpiperidine. Ramaswamy, S.; Scholze, M.; Plapp, B. V. *Biochemistry* **1997**, *36*, 3522. [c] Two formula units are present in asymmetric unit, with the second formula denoted by "A". [d] BTO = 3-butythiolane 1-oxide. Cho, H.; Ramaswamy, S.; Plapp, B. V. *Biochemistry* **1997**, *36*, 382. [e] Al-Karadaghi, S.; Cedergren-Zeppezauer, E. S.; Hövmoller, S.; Petratos, K.; Terry, H.; Wilson, K. S. *Acta Crystallogr.* **1994**, *D50*, 793. [f] Hydrogen-bonding involving coordinated perchlorate anion.

(25) (a) Perrin, D. D. *Dissociation Constants of Organic Bases in Aqueous Solution*; Butterworth: Markham, ON, Canada, 1965. (b) Braude, E. A.; Nachod, F. C. *Determination of Organic Structures by Physical Methods*; Academic: New York, 1955.

bond donor should be less, albeit the observation of identical Zn−O bond distances in **1·MeOH** and **2** is surprising. However, the results for the alcohol derivatives **1·MeOH** and **2** do suggest that the hydrogen-bonding interaction is probably more influential in determining the Zn−O(1) distance than is the slight difference in Lewis acidity of the zinc center present in the bmapa- versus bmpa-ligated complexes.

For the bmapa derivatives, the Zn−O(1) bond distance decreases with increasing donicity of the neutral oxygen donor ligand, with the methanol complex exhibiting the longest Zn−O(1) interaction (DN = 19; **1·MeOH**, Zn−O(1) 2.077(1) Å) and the TMSO derivative exhibiting the shortest Zn−O(1) bond (DN(value for DMSO) ≈ 29.8; **8**, $Zn-O(1)_{av}$ 2.035 Å). A consequence of the shortening to the Zn−O(1) bond in the series of complexes **1·MeOH** → **3**/**4** → **8** is that the neutral oxygen donor ligand is brought closer to the rigid primary amine hydrogen bond donor moiety of bmapa ligand. This leads to the formation of a tighter hydrogen-bonding interaction involving the zinc-bound oxygen atom of the donor in compounds **3**, **4**, and **8**, as compared to that found in **1·MeOH**, as evidenced by decreasing N(1)···O(1) heteroatom distances (Table 9). The relative strength of the hydrogen-bonding interactions in **1·MeOH**, **3**, **4**, and **8** may also be gauged by comparison of the vibrational frequencies of the asymmetric and symmetric vibrations of the primary amine unit in these complexes. As is shown in Table 9, complex **1·MeOH** exhibits the longest N(1)−H(1)···O(1) distance (2.92(1) Å) and the highest $\nu_{N-Hasym}/\nu_{N-Hsym}$ frequencies (3477, 3381 cm^{-1}), whereas **8** exhibits the shortest N(1)−H(1)···O(1) distance (av 2.82 Å) and the lowest $\nu_{N-Hasym}/\nu_{N-Hsym}$ frequencies (3434, 3342 cm^{-1}).

Our combined preliminary solution FTIR studies of formamide adducts **3**−**6** in CH_3CN and CH_3NO_2 solution suggest the presence of both free and bound formamide. On the basis of our complementary studies of the coordination properties of the bmapa-ligated zinc ion in these solutions, in the absence of any additional donor, we suggest that formation of equilibrium mixtures of **3**−**6** with either an acetonitrile adduct zinc complex (in CH_3CN) and free formamide, or a zinc−perchlorate complex (in CH_3NO_2) and free formamide, is occurring in solution. Unfortunately, these equilibria are not observable by ^1H NMR, as only a single set of formamide resonances is observed. This implies that displacement of the neutral donor from the zinc center by either CH_3CN or ClO_4^- is rapid on the NMR time scale. Efforts toward examining these equilibria using variable temperature FTIR are currently in progress. Of particular interest in these studies will be to attempt to correlate the position of equilibria involving formamide or sulfoxide binding with the observed ^1H NMR spectroscopic features associated with the primary amine donor of the bmapa ligand and the hydrogens of the neutral oxygen donor ligands themselves. For example, as outlined previously, the primary amine hydrogens of the bmapa ligand exhibit a downfield shift in CD_3CN spectra of **1**, **3**, **4**, **7**, and **8**, the magnitude of which is dependent upon the type of neutral oxygen donor present. This suggests differences in the solution hydrogen-bonding properties present in these complexes. Perturbation in the chemical shift position of the hydrogen atoms of the neutral donors between the bmapa- and bmpa-ligated systems, with the bmapa derivatives exhibiting a more significant downfield shift, also suggests an intriguing effect of the internal hydrogen bond donor in these systems that requires further exploration.

In conclusion, while this family of synthetic complexes does not exactly mimic the tetrahedral, NS_2-ligated zinc center found within the active site of LADH, we believe that, by using these systems, important chemical insight may be gleaned regarding the influence of a single hydrogen donor on the binding of a neutral oxygen donor molecule to a mononuclear zinc complex. From a broader perspective, as zinc sites in biological systems are known to mediate amide bond hydrolysis, the influence of hydrogen-bonding on the binding of formamides to a mononuclear zinc center expands the relevance of this work beyond just LADH to include the area of amide substrate activation.

Acknowledgment. We acknowledge the support of the Willard Eccles Charitable Foundation and the National Science Foundation (CAREER Award CHE-0094066).

Supporting Information Available: Tables listing FTIR, ^1H, and ^{13}C NMR data for **1**−**12** (Tables S1−S3). X-ray crystallographic files (CIF) for **1**−**6**, **7·DMSO**, **8**, **9·2DMSO**, **11**, and **12**. This material is available free of charge via the Internet at http://pubs.acs.org.

IC0255609